Developing an Imaging Biomarker to Detect Aberrant Brain Connectivity in Individual Patients

Esther Cox
Marquette University

DEVELOPING AN IMAGING BIOMARKER TO DETECT ABERRANT BRAIN CONNECTIVITY IN INDIVIDUAL PATIENTS

By

Esther Cox

A Thesis submitted to the Faculty of the Graduate School,
Marquette University,
in Partial Fulfillment of the Requirements for
the Degree of Master of Science

Milwaukee, Wisconsin

May 2017

ABSTRACT
DEVELOPING AN IMAGING BIOMARKER TO DETECT ABERRANT BRAIN CONNECTIVITY IN INDIVIDUAL PATIENTS

Esther Cox

Marquette University, 2017

Resting state functional MRI (rsfMRI) has been proven to be a valuable tool in clinical applications such as pre-surgical mapping, but there is not yet a functional and usable algorithm that can be used by physicians in a clinical setting to evaluate an individual patient for diseases and aberrant brain connectivity. If a physician wants to evaluate a patient in this way, the rsfMRI data must be looked at "by hand," i.e. the physician must manually evaluate the data and identify the functional ICN's and whether they are normal or aberrant. An algorithm that would automate this process and supplement the physician's evaluation would be very valuable and would decrease the time needed while increasing accuracy of the data analysis. The algorithm could be used in clinical applications as discussed, or academic and research applications to explore the neural basis of neurological disorders and deficits (epilepsy, etc).

rsfMRI data is significant for the proposed solution as it provides maps of functional brain connectivity within functionally specific neural networks, and those connectivity maps can help identify normal and abnormal brain conditions. Whether an ICA approach based on standard networks or an ROI seed based approach which utilizes temporal correlation is used, the end goal of this research is to develop and refine an imaging biomarker for aberrant brain connectivity. The biomarker algorithm should be able to detect the two main types of aberrant connectivity: increased (when abnormal brain connections are present) and decreased (when normal brain connections are missing). The algorithm should then correlate the connectivity patterns to a normative reference data set and create prioritized classification matches to that reference data set. This will allow identification of the aberrant connectivity patterns. Data from the Human Connectome Project (HCP) will be used to create the normative reference data set. The algorithm will finally be verified using simulated test data and test statistics.

ACKNOWLEDGMENTS

Esther Cox

The author wishes to thank Dr. Edgar DeYoe, Dr. Kristina Ropella, Dr. Brian Schmit, and Jedediah Mathis for their expertise and assistance. I would like to thank God, and also my husband and my family for their never ending encouragement, motivation, and support. I would like to thank the teachers and faculty of Marquette University, the Graduate School, and the Medical College of Wisconsin.

Data were provided [in part] by the Human Connectome Project, WU-Minn Consortium (Principal Investigators: David Van Essen and Kamil Ugurbil; 1U54MH091657) funded by the 16 NIH Institutes and Centers that support the NIH Blueprint for Neuroscience Research; and by the McDonnell Center for Systems Neuroscience at Washington University.

TABLE OF CONTENTS

LIST OF FIGURES

CHAPTER I

INTRODUCTION

Resting state functional MRI (rsfMRI) has been proven to be a valuable tool in clinical applications such as pre-surgical mapping, but there is not yet a functional and usable algorithm that can be used by physicians in a clinical setting to evaluate an individual patient for diseases and aberrant brain connectivity. If a physician wants to evaluate a patient in this way, the rsfMRI data must be looked at "by hand," i.e. the physician must manually evaluate the data and identify the functional ICN's and whether they are normal or aberrant.

An algorithm that would automate this process and supplement the physician's evaluation would be very valuable and would decrease the time needed while increasing accuracy of the data analysis. The algorithm could be used in clinical applications as discussed, or academic and research applications to explore the neural basis of neurological disorders and deficits (epilepsy, etc).

rsfMRI data is significant for the proposed solution as it provides maps of functional brain connectivity within functionally specific neural networks, and those connectivity maps can help identify normal and abnormal brain conditions. Whether an ICA approach based on standard networks or an ROI seed based approach which utilizes temporal correlation is used, the end goal of this research is to develop and refine an imaging biomarker for aberrant brain connectivity. The biomarker algorithm should be able to detect the two main types of aberrant connectivity: increased (when abnormal brain connections are present) and decreased (when normal brain connections are

missing). The algorithm should then correlate the connectivity patterns to a normative reference data set and create prioritized classification matches to that reference data set. This will allow identification of the aberrant connectivity patterns. Data from the Human Connectome Project will be used to create the normative reference data set. The algorithm will finally be verified using patient test data and test statistics.

The data used from the Human Connectome Project will represent actual patient data, however, for this thesis there will not be evaluation of an actual data set from an epileptic patient. The epileptic (aberrant) connectivity will be simulated in order to test the accuracy and noise sensitivity of the algorithm. Future work could continue with application of the algorithm to actual epilepsy patient data.

Finally for the purpose of this thesis, the following terms will be used. Magnetic Resonance Imaging will be defined as MRI, nuclear magnetic resonance as NMR, and resting state functional MRI as rsfMRI. ICA is independent component analysis, the method applied to the resting state MRI data to obtain the independent component networks (ICN), which represent the functionally connected areas of the brain. The data used is from the Human Connectome Project (HCP).

CHAPTER II

LITERATURE REVIEW

A. Magnetic Resonance Imaging

While the medical imaging technique of MRI has only become useful in a clinical setting relatively recently (within the past 30 years), the techniques and principles used in MRI have been developed over many more years and with contributions from many scientists (Geva, 2006). Indeed, "the scientists who made the extraordinary contributions … have led to five Nobel Prizes awarded to discoveries related to NMR/MRI" (Geva, 2006).

Among the scientists that contributed to the early development of MRI (i.e. before the phenomenon of nuclear magnetic resonance, or NMR, was discovered) are Jean Baptiste Joseph Fourier, Nikolas Tesla, and Sir Joseph Larmor. Although their discoveries and methods were made before NMR was known, they are critical to the measurement and analysis of MRI even today. The mathematical method of the Fourier transform that was developed by the French mathematician Jean Baptiste Joseph Fourier is critical to the creation of magnetic resonance images. Without it, the frequency and phase information contained in the raw NMR data could not be analyzed and image reconstruction would not be possible (Geva, 2006). Nikola Tesla was a Serbian-American inventor and researcher who had over 700 patents in the United States and Europe, and he "discovered the rotating magnetic field, the basis of most alternating current machinery" (Roguin, 2004). The Tesla, named after Nikola Tesla, is the SI unit of magnetic flux density, and is used in MRI as the measure of the strength of the applied magnetic field.

Sir Joseph Larmor was an Irish physicist who was the first to calculate the rate at which energy is radiated by an accelerated electron (Tubridy, 2000; Geva, 2006). The Larmor equation (named after him), is important in MRI because the Larmor frequency is the frequency at which a proton precesses when placed into an external magnetic field. The Larmor equation is $\omega = \gamma B_0$ where ω is the precession frequency, γ is the gyromagnetic ratio, and B_0 is the applied external magnetic field (Nishimura, 1996). The foundation of mathematics, physics, and engineering that was begun by these three scientists is what modern MRI was built upon today.

As research continued into the modern era, an Austrian born scientist named Isidor Rabi began research into the magnetic properties of crystals and atomic nuclei in 1929 and 1930 (Geva, 2006). He set up a molecular beam lab and in 1931 and began working on determining the nuclear spin and magnetic moment of sodium (Chodos, 2006). Eventually, as he continued his work on the problem, Rabi improved his methods and developed the magnetic resonance method, which is the basis of MRI. The method discovered that atomic magnetic moments align in an external magnetic field and then spin (precess) about the direction of the magnetic field at the Larmor frequency, which depends on the strength of the external magnetic field and the gyromagnetic ratio (Chodos, 2006). Ultimately, this led to Rabi predicting in 1937 that "the magnetic moments of nuclei in these experiments could be induced to flip their orientation if they absorbed energy from an electromagnetic wave of the right frequency. They would also emit this amount of energy in falling back to the lower energy orientation" (Chodos, 2006). Once this discovery was made, the molecular beam was modified so a radio frequency signal was applied to the beam to tune it to produce resonance. The resonance

was first observed in 1938, and Rabi was awarded the Nobel Prize in 1944 for his work (Chodos, 2006). Ultimately, the combination of the previous decades of work from this group of dedicated scientists culminated in the first MRI exam on a live human patient which occurred on July 3, 1977 (Chodos, 2006)

A very simple description of how MRI works is as follows: the patient enters the scanner, and a radio wave is sent in. Then, the radio wave is turned off and the patient emits a signal, and finally the signal is received and sampled and the picture is reconstructed. However, the physics and details of how MRI works certainly deserve a more thorough examination. Much of the following information on magnetic resonance imaging can be found in the book Principles of Magnetic Resonance Imaging by Dwight G. Nishimura (Nishimura, 1996).

First of all, it is important to know that biological tissue can be magnetized. Spinning charged particles create an electromagnetic field, and for the purposes of MRI the interest is in the charged nuclei of atoms that are present in the human body. Specifically, MRI uses the charged hydrogen nucleus. Each of these hydrogen nuclei produces a small magnet as it spins, and when these hydrogen "magnets" are placed into an external magnetic field they align. The hydrogen nuclei can align in either a parallel or an antiparallel state. When they are in the parallel state, they are in a low energy state, and when they align antiparallel, they are in a higher energy state. There are slightly more hydrogen protons in the lower energy state, and although there is only a very small amount more, that difference is enough for the biological tissue to become magnetized. This initial magnetization of the biological tissue is traditionally known as M_0. However, M_0 can't be measured as is because the net magnetization is in the same direction as the

applied magnetic field (known as B_0). In order to make the net magnetization of the tissue useful, a radio frequency (RF) excitation pulse (traditionally called B_1) is applied. The pulse B_1 is applied in the transverse plane and is applied at a frequency that matches the Larmor frequency of the hydrogen protons. Since the RF pulse is applied at the Larmor frequency, the protons will resonate at this frequency and energy will be added to the protons. The RF pulse is brief, and once it ends the protons will begin to spin (precess) out of the higher energy state and back to their original state. The added energy from the RF pulse will cause the random precessions to align, and this produces a magnetic resonance signal in the transverse plane that can be measured and used to reproduce an image. This phenomenon is shown visually in Figure 1.

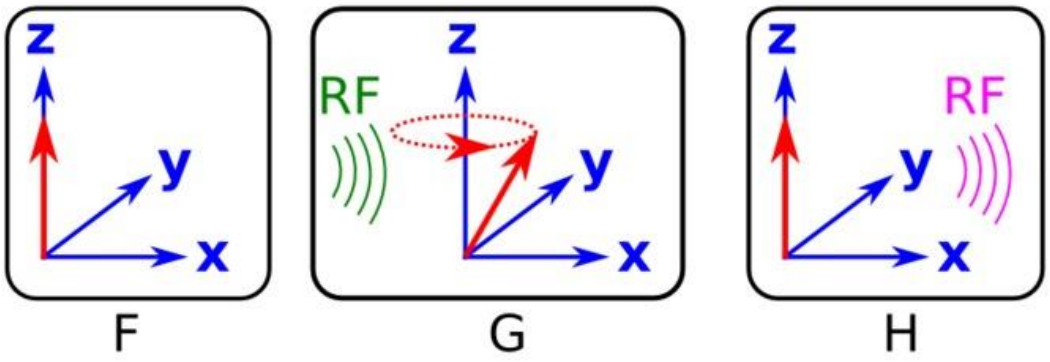

Figure 1: Figure F shows the aligned protons in the biological tissue that produces the net magnetization M0. Figure G shows the applied RF pulse that provides energy to the system and causes the protons to precess about the z axis at the Larmor frequency. Figure H shows the precessing protons returning to their equilibrium (lower energy) state, emitting a signal in the XY plane that can be measured by a receiver coil (Dimmock, 2013).

In addition to the main external magnetic field and the applied RF pulse, a gradient magnetic field (G) is also applied. The purpose of this gradient field is to change

the value of B_0 at different locations along the patient. This in turn changes the Larmor frequency across the volume, so at every location the precession frequency of the protons is different. This is absolutely critical to image reconstruction because with the gradient field, frequency maps to location (i.e. if we know the frequency we know the location of the slice within the volume). This allows for slice selective excitation, and it also allows frequency encoding in one direction and phase encoding in the other direction. In practice, a signal bandwidth is used for the RF pulse so that a slice of selected thickness will resonate. A smaller width produces a higher image resolution but has a lower signal since fewer protons will be resonating. The slope of the gradient also affects the slice thickness, with a steeper gradient slope producing a narrower slice. To get a sharply defined image slice, a rectangular shaped RF pulse (in the frequency domain) is needed. Even to this day, the quality of the gradient remains an issue. The more linear the gradient is, the better for image quality, but there are many factors that influence the linearity of the field. Even just the person laying inside of the scanner will affect the linearity of the gradient because they change the magnetic field.

As discussed earlier, the signal measured is in the transverse plane and is measured by a receiver RF coil. This receiver coil is often the same as the one that applies the RF pulse, and it measures the signal as current given off by the precessing protons. The signal is phase encoded in the y direction by the y direction gradient field G_y and frequency encoded in the x direction by the x direction gradient field G_x. As the data is received by the coil, it is received in k space, an abstract concept where the raw MRI data is stored before the Fourier transform is applied. Each of the received samples is a data point in k space, so when all the data is obtained you end up with a raw data matrice

that represents the spatial frequency of the signal. The center of the k space matrice is not the center of the image (k space does not correlate to spatial location within the image). Instead, the center of k space represents the amount of time the image changes slowly in space. This means that the edges of k space contain the fine details of the image, or the rapid changes across space, while the center of k space contains the coarser details of the image, or the slower changes across space. Finally, in order to transform the data from k space to image space (to reconstruct the image), the 2D Fourier Transform (2DFT) is applied to the data. The 2DFT transforms the data from frequency space to image (spatial) space, allowing reconstruction of the true image.

B. Functional Magnetic Resonance Imaging

In order to understand resting state functional Magnetic Resonance Imaging (rsfMRI), functional MRI (fMRI) must first be explained. fMRI is a method of MRI that developed in the 1990s and is a way to measure brain activity and function. According to Dr. Seiji Ogawa, who is credited as one of the discoverers of fMRI, "the most widely used method is based on BOLD (Blood Oxygenation Level Dependent) signal change that is due to the hemodynamic and metabolic sequelae of neuronal responses" (Ogawa & Sung, 2007). fMRI is based on the fact that the human brain is organized spatially so that specific functions of the brain are localized at various sites (Ogawa & Sung, 2007). That localized functionality is what allows fMRI to locate areas of the brain and map them spatially, along with the physiological basis of the BOLD signal.

The BOLD effect in MRI functions is based on the hemoglobin molecule. In 1936, Linus Pauling and Charles Coryl discovered that de-oxygenated hemoglobin is

paramagnetic and oxygenated hemoglobin is diamagnetic (Pauling & Coryl, 1936). This causes a difference in the magnetic susceptibility between blood and the surrounding tissue, and the water protons in the area around the blood sense the field distortions caused by the change in magnetic susceptibility, and they reflect the signal decay process (or precession as discussed earlier) (Ogawa & Sung, 2007). Thus, when the amount of deoxygenated hemoglobin in the blood changes, the relaxation of the water molecules changes, and these changes can be seen in the MRI image as variation in image intensity (Ogawa & Sung, 2007).

The term blood oxygenation level dependent (BOLD) contrast was developed by Ogawa, Lee, Kay, and Tank in 1990 and applied to magnetic resonance imaging techniques (Ogawa, Lee, Kay, & Tank, 1990). Ogawa et al. demonstrated that

> Since BOLD contrast depends on the state of blood oxygenation, physiological events that change the oxy/deoxyhemoglobin ratio should lend themselves to noninvasive detection through the accentuation of BOLD contrast in gradient-echo proton images at high magnetic fields (p. 9868).

Put simply, increased neural activity in specific functional areas of the brain occurs as a person performs tasks, requiring increased blood flow to those activated areas and ultimately providing the BOLD signal that is measured by fMRI.

fMRI data is traditionally collected by having the patient perform a specific task to activate a specific functional area of the brain. For example, the patient is asked to tap their fingers in a specific order in order to activate the motor cortex (i.e. to cause the increased blood flow that will lead to the BOLD signal), and the fMRI is able to measure the signal change and identify the motor cortex. Today, fMRI based on the BOLD signal is widely used to evaluate the neural basis of various functional parts of the brain, such as the sensorimotor and mental processes (Ogawa & Sung, 2007). One of the most

significant outcomes of fMRI that relates to this work is the functional brain maps that have been developed from fMRI. By providing specific stimuli to the patients, Shirer, Ryali, Rykhlevskaia, Menon, and Greicius were able to decode 90 different functional regions of interest (ROIs) (Shirer et al., 2011) as shown in Figure 2.

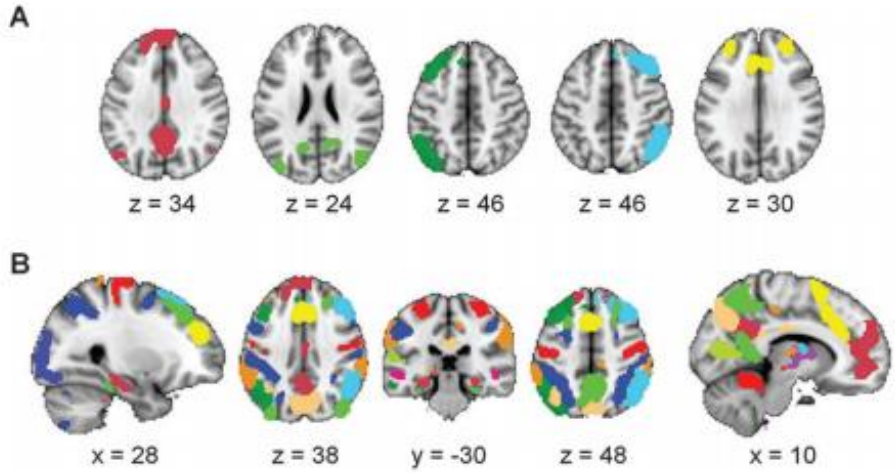

Figure 2: Functional parcellation of the brain into 90 ROIs that cover the majority of cortical and subcortical gray matter (Shirer et al., 2012). Row A shows 5 of the 90 ROI's, and Row B shows the 90 ROIs overlaid on a brain, demonstrating that a majority of the gray matter is covered (Shirer et al., 2012).

These functional areas can be used to define which parts of the brain do what in the body, for example, which of the ROIs control the motor functions, which control the visual functions, etc. This is important for the research described in this thesis because it allows selection of only the areas of interest, in this case the medial-temporal lobe(s) that are affected by epilepsy.

C. Resting State fMRI

Continuing to build on the base of MRI and fMRI, Bharat Biswal discovered what would ultimately come to be known as resting state fMRI (rsfMRI). Together with his

colleagues, Biswal discovered that there is a high temporal correlation between low frequency fluctuations of resting brain functional regions (Biswal, Yetkin, Haughton, Hyde, 1995). The data showed that the time course in the sensorimotor cortex highly correlated to other areas of the brain associated with motor function, even when the subjects were at rest (i.e. not performing a task as in traditional fMRI) (Biswal, et al., 1995). This was a groundbreaking discovery "suggesting ongoing information processing and ongoing functional connectivity between these regions during rest (van den Heuvel et al., 2010). Figure 3 shows the temporal correlation compared to the traditional task-activated response of fMRI for a component localized to the motor cortex. Biswal continued to build on the concept, further demonstrating the presence of BOLD and flow-weighted frequency variations that, when used to weight the connectivity, result in a much improved resting state functional connectivity map (Biswal, et al., 1997). In this study "the resting state time series of a voxel in the motor network was correlated with the resting state time series of all other brain voxels, revealing a high correlation between the spontaneous neuronal activation patterns of these regions" (van den Heuven, et al., 2010). This concept is shown visually in Figure 3.

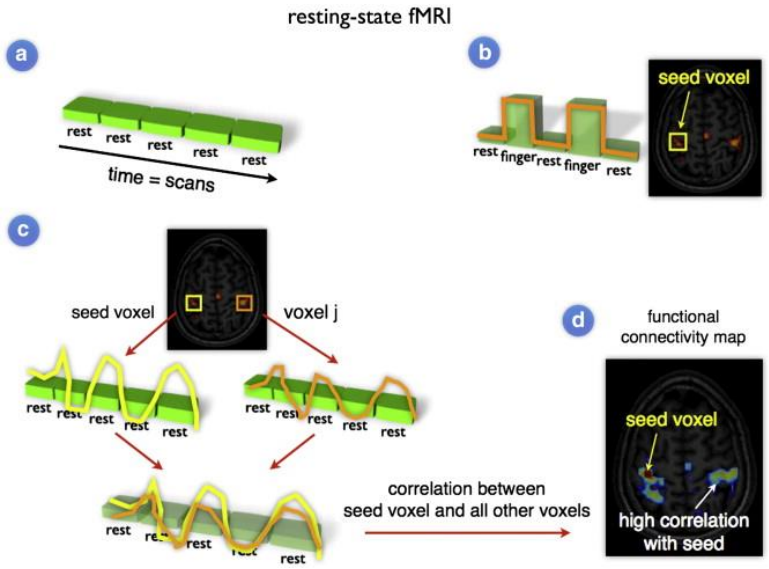

Figure 3: "Resting-state fMRI studies are focused on measuring the correlation between spontaneous activation patterns of brain regions. Within a resting-state experiment, subjects are placed into the scanner and asked to close their eyes and to think of nothing in particular, without falling asleep. Similar to conventional task-related fMRI, the BOLD fMRI signal is measured throughout the experiment (panel a). Conventional task-dependent fMRI can be used to select a seed region of interest (panel b). To examine the level of functional connectivity between the selected seed voxel i and a second brain region j (for example a region in the contralateral motor cortex), the resting-state time-series of the seed voxel is correlated with the resting-state time-series of region j (panel c). A high correlation between the time-series of voxel i and voxel j is reflecting a high level of functional connectivity between these regions. Furthermore, to map out all functional connections of the selected seed region, the time-series of the seed voxel i can be correlated with the time-series of all other voxels in the brain, resulting in a functional connectivity map that reflects the regions that show a high level of functional connectivity with the selected seed region (panel d)" (van den Heuven et al., 2010).

The high temporal correlation that is graphically displayed as time course in Figure 3 can also be seen in Figure 4 in the spatially related region of the brain (in this case the sensorimotor cortex)

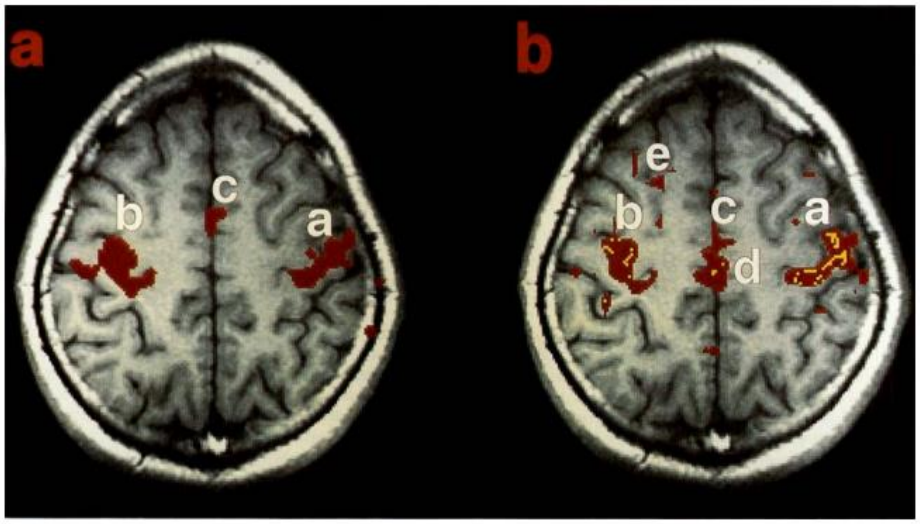

Figure 4: a) Traditional fMRI task-activated response in the sensorimotor cortex due to left and right finger movement. b) The fluctuation response with the brain at rest from the temporal correlation discovered by Biswal et al. (Biswal et al., 1995). In this figure, red is a positive correlation and yellow is negative.

This demonstrates again that there is spontaneous brain activity during a resting state that is correlated between functionally related brain regions to create functional connectivity maps, which is the basis of rsfMRI (van den Heuven et al., 2010).

One of the most significant benefits to rsfMRI is that the patient does not need to perform a specific task in order to obtain the functional connectivity map. The need for movement or another active task in task based fMRI can introduce motion artifact. For example, with fMRI if the area of the motor cortex that operates the legs needs to be isolated, the patient must move their legs in some way. This makes it very difficult to keep the head as still as required for an MRI. Thus, rsfMRI eliminating the need for a task holds many advantages, including for patients that may have a difficult time completing certain tasks, such as small children, the elderly, and epilepsy patients (very significant in this research).

D. Post Processing of rsfMRI Data

The data produced from rsfMRI can be processed in several ways. One of these methods is the seed based method where the connectivity is based on a predefined brain region known as a seed that is obtained from an activation map or a task based scan (van den Heuven et al., 2010). However, there are methods that do not require a seed in order to perform the classification. One of the most common of these methods and the one used to analyze the data used in this research project is Independent Component Analysis (ICA). A detailed explanation of the mathematical working of ICA can be found in Independent component analysis, A new concept by Pierre Comon (Comon, 1992). This method works by "attempting to separate independent "sources" that have been mixed together", such as separating voices as was applied by Bell and Sejnowski in 1995 (Bell, Sejnowski, 1995; Calhoun, Adali, Pearlson, Pekar, 2001). When applied to rsfMRI data, it can be used to separate temporally independent sources, which is ideal since the correlations in rsfMRI data are temporal in nature (Calhoun et al., 2001). This was first done by Biswal and Ulmer in 1999 when they applied ICA to rsfMRI data. The results showed that ICA can reliably separate the temporal signal sources from the noise and determine the location of said signals (Biswal, Ulmer, 1999). Figure 5 shows some of the separated components from the ICA analysis.

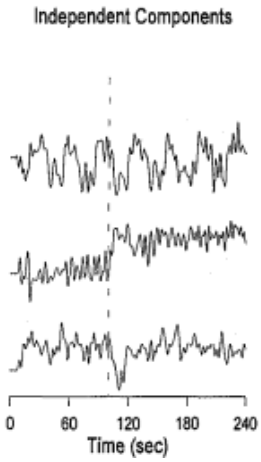

Figure 5: The first 3 separate ICA components from the MRI data (Biswal, Ulmer, 1999)

Further studies continued to validate the reliability of ICA when used to separate functional components of the brain from rsfMRI data. Van de Ven et al showed that spatial ICA yielded connectivity maps that were consistent both within and between subjects (Van de Ven, Formisano, Prvulovic, Roeder, Linden, 2004). Subjects were told to lie at rest in the MRI scanner and keep their eyes open to obtain the resting state data, and then the ICA analysis was performed on the MRI data, decomposing the datasets into components of interest (COIs) (Van de Ven et al., 2004). Figure 6 shows the top 3 components of interest obtained from one of the subjects.

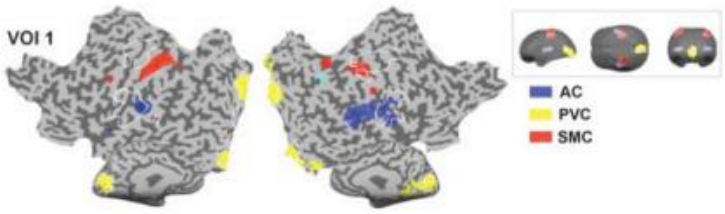

Figure 6: The top 3 components of interest separated out from the rsfMRI data by ICA (Van de Ven et al., 2004)

De Luca et al and Beckmann et al further showed that the individual components that contribute to the rsfMRI data can be reliably separated and identified by ICA (De Luca, Beckmann, Stefano, Matthews, Smith, 2005; Beckmann, DeLuca, Devlin, Smith, 2005). It is also important to note that in a real physiological rsfMRI data set, both noise and the correlated random signals (i.e. the signals that are the source of the correlation) are present, and an accurate simulated component will include the noise.

E. Using rsfMRI in a Clinical Setting

rsfMRI is important to the research world as it provides important information about both the healthy brain and various disease types (Lee, Smyser, Shimonya, 2012). However, its use in a clinical setting is only beginning to be explored. One of the most common clinical applications is presurgical planning for patients with brain tumors as shown in Figure 7 (Lee et al., 2012).

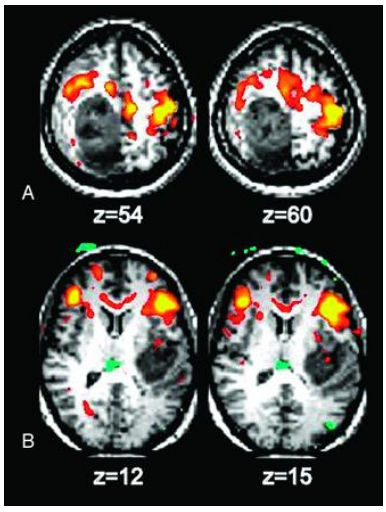

Figure 7: The motor and language functional areas in 2 patients. A) The somatosensory area can be seen as displaced due to the tumor. B) The Broca area is displaced due to the tumor (Lee et al., 2012).

The method can also be used for presurgical planning in epilepsy patients. Lui et al was the first to locate sensorimotor areas using rsfMRI in patients with epilepsy (Lui et al., 2009), and further research continued to validate the rsfMRI data can be used to identify epileptic centers (Lee, 2012). Newer research has shown that rsfMRI has potential to be used to perform research and develop a deeper understanding of the neurological basis of Alzheimer disease, psychiatric diseases, depression, autism, schizophrenia, ADHD, and other neural diseases that have previously been difficult to diagnose (Lee et al., 2012). However, there are challenges that must be overcome before clinical applications are practical. The most prevalent is that it is difficult to accurately research clinical diseases and problems in individual patients (as opposed to groups of patients) (Lee et al., 2012). This is where the research presented in this thesis becomes important as the biomarker algorithm developed here will help advance rsfMRI research towards relevant clinical applications for individual applications (to be discussed further in Section G).

F. Evaluating Groups of Patients

Evaluating groups of patients holds promise in a clinical setting because combining multiple data sets and "jointly estimating the common functional networks is more robust" (Liu, Awate, Fletcher, 2012). Traditionally, this is done by identifying each patient's common networks, and then combining them together to draw group inferences (Liu et al., 2012). Liu et al demonstrated that a stable and consistent group connectivity map can be produced (Liu et al., 2012), and Beckmann et al similarly showed successful group analysis (Beckman, Mackay, Filippin, Smith). Beckman et al analyzed the data as

shown graphically in Figure 8, by concatenating all of the subject's data sets and then applying ICA to identify the resting state connectivity patterns present in the entire group (Beckmann, et al).

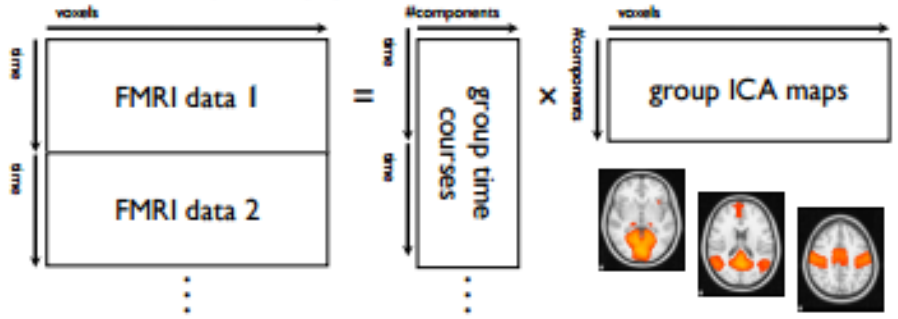

Figure 8: The multiple sets of individual patient data are concatenated into a group data set, and then the ICA analysis is run to obtain a group ICA map of all of the common functional connectivity maps present in the entire group.

The rsfMRI group data cannot simply be averaged because the time course of each person is unique and random. Thus the approach in Figure 8 makes it possible to perform a group analysis from the individual patient's raw data. This group analysis is useful for looking at trends across large groups of patients, for example, to investigate the maps that are present in healthy individuals (as a group) verses diseased patients (as a group). While this is important in disease research and advancing rsfMRI analysis, it is not as useful in a clinical setting as a single subject evaluation. In order to be truly useful, a clinician must be able to analyze one single patient for their specific connectivity patterns and changes within that pattern due to disease.

G. Single Subject Evaluations

As already mentioned briefly, individual subject rsfMRI data must be evaluated accurately in order to be truly useful in a clinical setting, and this is where the research presented in this thesis becomes important. Currently in this area, research has been done investigating the within subject test-retest reliability (reproducibility) and the between subject variation by Chou et al (Chou, Panych, Dickey, Petrella, Chen, 2012). They performed 9 resting state scans over 1 year and calculated the within subject reproducibility and the between subject variation. The data showed a long term within subject test-retest reproducibility of >70%, however, it also showed a significant between-subject variation (Chou et al., 2012). The significant variation is what makes it difficult to evaluate a single subject, especially without a functional classification algorithm that a clinician can use. Despite this difficulty, there are multiple studies and methods as described in Section D that continue to build the clinical credibility of rsfMRI when evaluating individuals, but there is still no functional and usable algorithm that clinicians can use to easily check individual patient data for aberrant connectivity patterns that may signal disease. The purpose of this research is to begin development of such a clinical tool.

H. Medial Temporal Lobe Epilepsy

In order to evaluate the approach developed here as a clinical tool, a patient with an aberrant connectivity pattern must be compared to a normative database. In this research, the chosen aberrant connectivity is due to medial (mesial) temporal lobe epilepsy (mTLE). Research has shown that patients with medial temporal lobe epilepsy have an aberrant connectivity pattern in the medial temporal lobe of the brain. In a study

by Wei Liao et al., 18 patients with mTLE were compared to 27 healthy controls. The mTLE patients showed increased connectivity within the medial temporal lobes and between the parietal and frontal lobes (Liao et al., 2010). These lobes are highlighted in Figure 9.

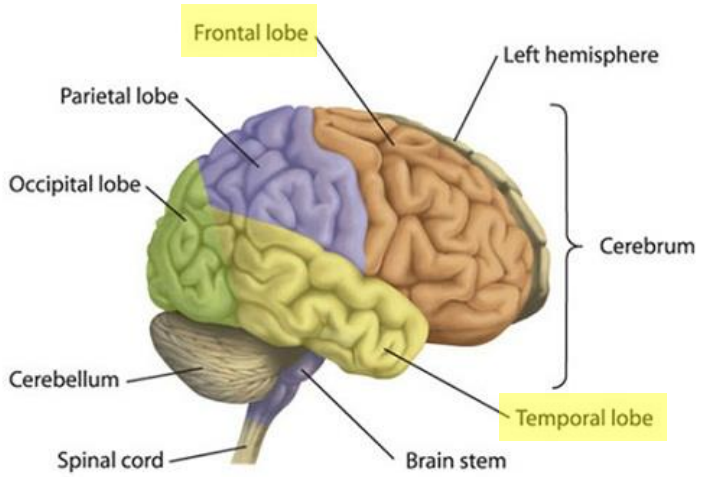

Figure 9: The frontal and temporal lobes affected by mTLE (humandiagraminfo.com).

Since the medial temporal lobe and frontal lobe are those affected by mTLE, a synthetic aberrant connectivity pattern will be created that simulates the abnormal connectivity between these lobes. The creation of this simulated aberrant connectivity pattern will be discussed in further detail in Chapter 3, Section C.

CHAPTER III

METHODOLOGY

A. Human Connectome Project Data

The data used in this research was obtained from work done by a consortium of 10 institutions led by Washington University, University of Minnesota, and Oxford University (Van Essen et al., 2012). The 5 year project is titled the Human Connectome Project (HCP), and its purpose is "comprehensively mapping human brain circuitry in a target number of 1200 healthy adults" (Van Essen, 2016). The HCP data is collected using 4 different imaging modalities, including rsfMRI, on new 3T and 7T MRI scanners. The scanning took place at Washington University over a 2 day period (for each subject). Scans from 1200 healthy adults were collected and include both the resting state scans and anatomical T1 weighted and T2 weighted scans (Van Essen et al., 2012). Figure 10 shows the schematic outline for the data collection process of the HCP.

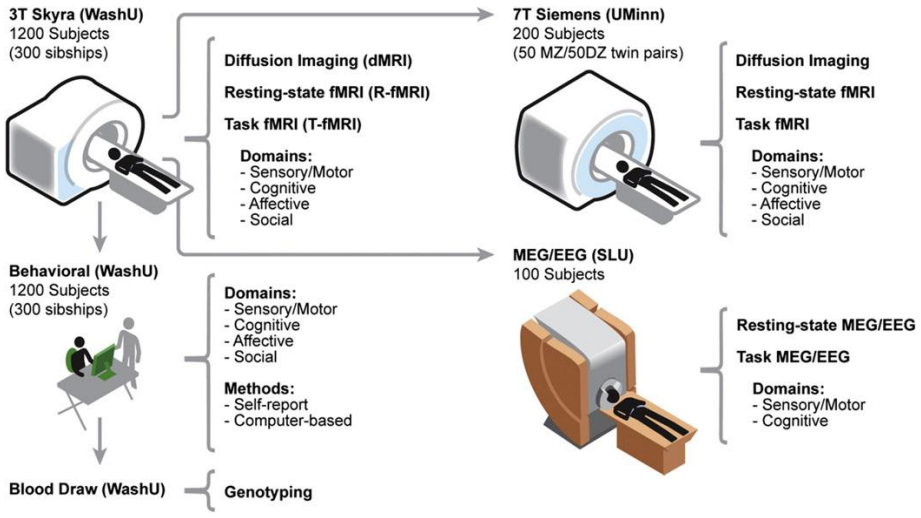

Figure 10: The schematic outline for the HCP project data collection (Van Essen, et al., 2012).

The scans at Washington University were performed on a "customized 3T Connectome scanner adapted from a Siemens Skyra" (Van Essen, et al., 2012), and 200 of the subjects had additional scans performed with a customized 7T scanner at the University of Minnesota. The data collection was performed on 2 separate scanners to optimize the MR image data quality. According to The Human Connectome Project: A data acquisition perspective published by David Van Essen et al., "3T systems are the more mature and robust platforms, compatible with the need to scan a large number of subjects. 7T systems offer advantages, especially for the resting and task-based fMRI studies […] however, 7T platforms are less mature and more challenging to work with, and are thus incompatible with an ambitious data collection strategy" (Van Essen, et al., 2012). This resulted in the dual strategy used in the data collection. The customized 3T scanner, used to scan all 1200 subjects, was specially designed by the consortium with unique gradients and RF hardware. The gradients had higher amplitudes that served to increase SNR, and the RF hardware allowed parallel imaging, drastically reducing the acquisition times (very important due to the high volume of subject data that was collected) (Van Essen, et al., 2012). Exhaustive information on the specifics of the scanners, pulse sequences, and data collection process can be found in The Human Connectome Project: A data acquisition perspective (Van Essen, et al., 2012).

The first data release included data from 900 subjects, and is open access to those in the scientific community that register and agree to Open Access Data Use Terms. The data used in this research was this first release open access data, and obtained through work done by Dr. Edgar DeYoe at the Medical College of Wisconsin. The data are de-

identified so no IRB approval was needed for the lab to obtain and use the data. Individual subject data sets are identified only by a unique number (not correlated in any way to subject identity), and no other personal identifying information is included in the data.

The individual subject data used to create an aberrant connectivity data set (to be discussed further in Chapter 3, Section C) were chosen by manually examining the results of an independent component analysis (ICA) analysis of the HCP data and choosing network components that had good activation in the brain regions of interest in mesial temporal lobe epilepsy (Chapter 2, Section G). The ICA analysis was performed with the MELODIC software package (Jenkinson, 2013) which yields the connectivity patterns among different brain regions. The ICA networks from the analysis were then compared to a known brain map, and the subjects with good activation in the areas of interest were chosen as the base dataset to which aberrant synthetic signals were to be added (described below, section C).

B. Creating the Normative Data Set

After the HCP data were obtained, the first step was creating a normative data set to which patterns of potentially aberrant connectivity could be compared. The schematic outline of the processing to create the group average for 3 subjects is shown in Figure 11, and the exact AFNI script used to accomplish this is attached in Appendix A. In order to create this normative set, 3 subject data sets were chosen at random. The data sets were co-registered to the MNI 152 human brain atlas, created by John Mazziotta, et al through the International Consortium for Brain Mapping (Mazziotta, et al., 2001). Next, they

were processed through the Melodic ICA analysis (Biswal, et al., 2012; Calhoun, et al., 2001) and for each of the 3 subjects, the independent component networks (ICN's) that represented auditory, default, motor, and vision networks were manually identified by visually comparing the ICN's to a published brain connectivity map (Shirer, et al., 2012). Next, the selected ICN's from all 3 subjects were spatially averaged together to create a group average data set (and this process was repeated for each of the 4 different functional ICN's). The averaging was performed with AFNI commands (including 3dCalc), and the final group average data set consisted of the average ICNs for each of the 4 functional networks.

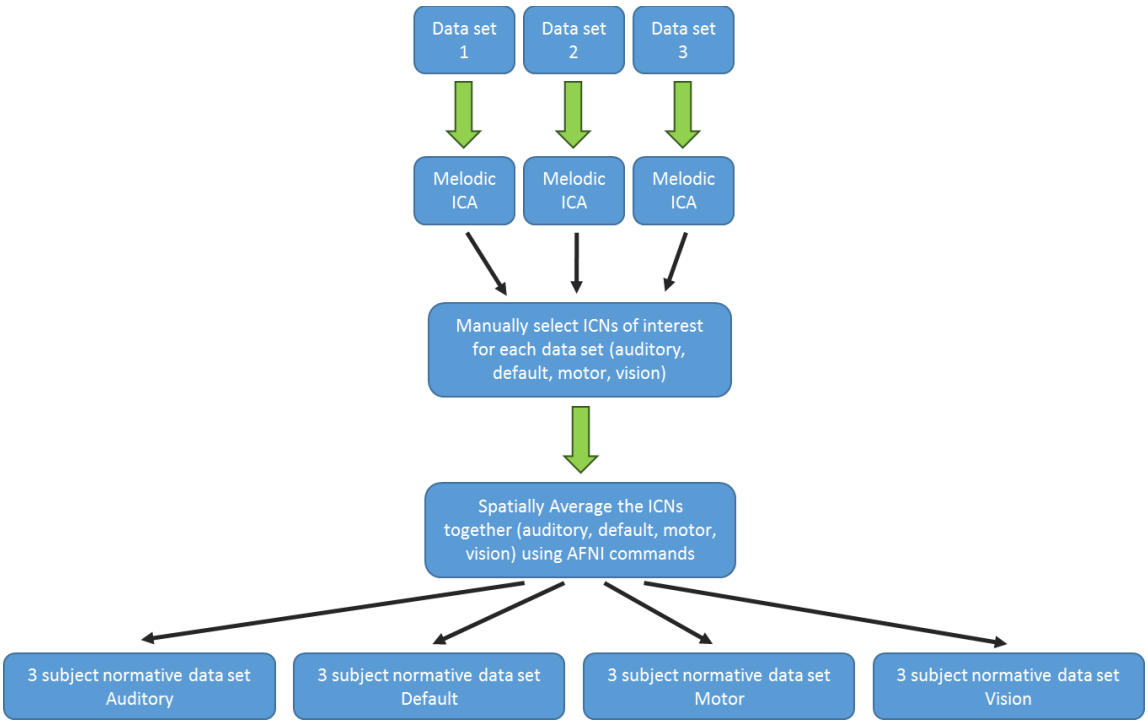

Figure 11: The schematic of the process used to create the normative data sets for the auditory, default, motor, and vision ICNs.

C. Creating Simulated Aberrant Connectivity

Functional connectivity is broadly "defined as statistical dependencies among remote neurophysiological events" (Friston, 2011), and in the case of rsfMRI, the statistical correlation is due to the temporal (time course) correlation between the voxels in different brain regions (this is further detailed in Chapter II, Section C). Thus, adding the same time course to a set of otherwise uncorrelated voxels will ultimately simulate functional connectivity. Our goal was to do this for a set of voxels within the medial temporal and frontal lobes, thus creating a simulated pattern of aberrant connectivity that might plausibly be found in medial temporal lobe epilepsy (mTLE) patients. The step by step process used to create the simulated aberrant connectivity pattern is outlined in Figure 12.

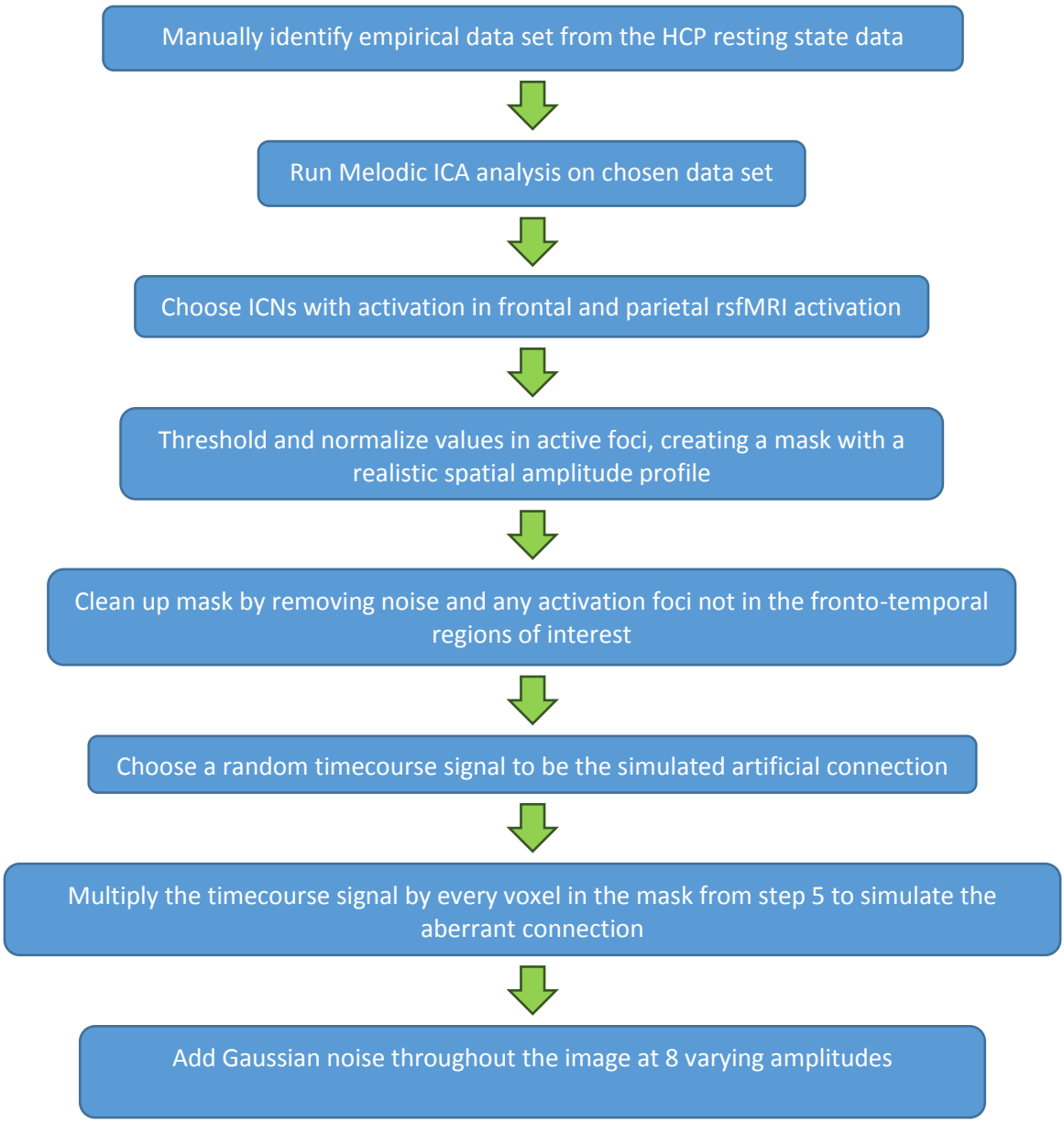

Figure 12: Schematic of process used to create simulated aberrant connectivity.

In order to create simulated aberrant connectivity patterns that mimic those that might be in mTLE patients, the areas of the medial temporal lobe and frontal lobe affected by mTLE were identified manually as per the literature (Shirer, et al., 2012). The first step was to create a brain mask containing the set of voxels that were to be aberrantly connected. To make this mask, we randomly chose an empirical data set from

the HCP resting state data and ran the Melodic ICA analysis. ICNs containing voxels from the frontal and parietal cortex having strong resting state activation were selected and added together using the 3dcalc function in AFNI. Then, the combined resting state data were thresholded to isolate a subset of voxels that normally have strong resting state activation, thus providing a physiologically plausible set of voxels that might be aberrantly connected in mTLE. The resting state connectivity values (correlations) of the responsive voxels were then normalized to a range of 0 to 1.0. This created a mask with spatially realistic amplitude profiles within the activation foci and zero values everywhere else. The spatially varying amplitude is important in order to provide the aberrant connectivity signals with a physiologically plausible pattern within the brain (i.e. the signals within the centers of simulated regions of connectivity will be higher than at the edges). This is illustrated for several foci of activation in Figure 13.

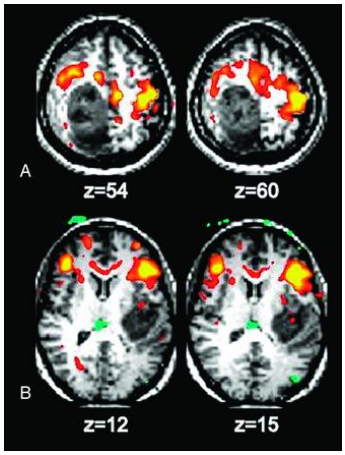

Figure 13: A representation of the physiological amplitude variation where yellow represents higher correlation and red represents lower correlation (Lee, et al., 2012)

Finally to complete the mask, the draw tool in the AFNI image viewer was used to clean up the mask created in the previous step in order to eliminate unwanted noise and any foci that were not within the lobes of interest in mTLE (frontal and temporal).

To create the simulated aberrant connectivity (temporal correlation across voxels), a resting state fMRI timecourse was chosen at random. Figure 14 shows such a time course and its powerspectrum. To create the artificial pattern of aberrant connectivity, the selected timecourse vector was multiplied by the amplitude scale factor for each voxel in the mask dataset described above. This then yielded a "3D plus time" volumetric dataset consisting of the scaled random timecourse within the voxels comprising the activity foci of the aforementioned mask and a zeroed timecourse everywhere else.

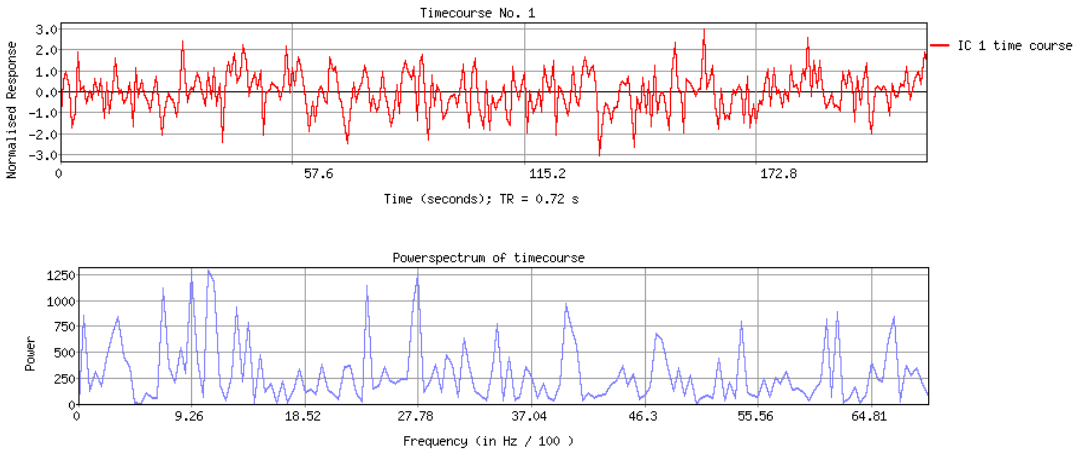

Figure 14: Example of resting state fMRI time course (upper panel) and its powerspectrum (lower panel) that was added to target voxels to simulate aberrant functional connectivity.

D. Simulated fMRI Noise

The next step in creating the simulated aberrant connectivity was to add Gaussian noise.

Noise was added because real physiological brain connectivity signals always occur with some level of noise. The resulting signal for voxel 'i' is expressed by Equation 1 (Beckmann et al., 2005).

$$x_i = A_{si} + n_i \quad (1)$$

x_i represents the signal measured at a specific voxel location (i) which is the sum of A_{si} and n_i, where A_{si} represents the correlated random signal in that voxel, and n_i represents Gaussian noise at that voxel (Beckmann et al., 2005). To realistically simulate the noise component n_i, a different unique sample of Gaussian noise was added to each voxel throughout the entire brain using an AFNI function that generates the noise and adds it to the aberrant connectivity signal. Eight amplitudes of the Gaussian noise were added to the simulated connectivity signals in order to test the effectiveness of detecting aberrant connectivity as a function of signal to noise ratio, which ranged from 1.0 to 47.

Equation 2 is the final signal equation for the simulated aberrant connectivity and includes all the factors used to compute the final signals that comprise the simulated aberrant connectivity data set:

$$x_i = m_i * A_{si} + S * n_i \quad (2)$$

where x_i again represents the total signal at a specific voxel location (i). A_{si} is the correlated random signal created by adding the time course, but in the final signal it is multiplied by m_i, the ROI mask that varies in amplitude from 1 at the center to 0 at the edges to make the spatial profile of activation more physiologically plausible. Finally, the noise n_i is multiplied by the scaling factor S to vary the Gaussian noise amplitude to 8 different levels to allow testing with multiple Signal to Noise ratios.

E. The Biomarker Algorithm

The biomarker algorithm is a clinical tool that clinicians can use to evaluate if an individual patient's connectivity pattern matches that of the normal population. To do this, the individual patient's connectivity must be compared in an objective way to the normative database, and a quantitative evaluation of how well they match must be returned to the clinician. The clinician can then decide based on the quantitative value the next steps to take for each individual patient. This will reduce or eliminate the need for the clinician to manually look at each patient's connectivity patterns and try to identify qualitatively if there is an aberrant pattern. The method of comparison that will be used to do the evaluation is the Dice coefficient.

The Dice coefficient is a statistical verification method that has become one of the more reliable comparison methods used in MRI research (Zou et. al., 2004). It was developed by Lee Dice to compare the degree to which 2 species are related in nature (Zou, et al, 2004). The Dice coefficient is a measure of the spatial overlap accuracy of 2 images, in this case the patient connectivity pattern(s) and the normative connectivity patterns. The value of the Dice coefficient ranges from 0, which means there is no spatial overlap, to 1, meaning the images overlap completely (Zou, et. al., 2004). This method is useful for the comparison between patients with aberrant connectivity and a normative data set because it can spatially compare the degree to which the activated voxels in the aberrant data set match the activated voxels in the normative data set, and return a coefficient that is a reliable quantitative measure of how well they match. The Dice coefficient is calculated by Equation 3

$$\text{Dice}(A,B) = 2(A \cap B)/(A+B) \quad (3)$$

where A and B are the data sets being compared and ∩ is the intersection. Put simply, Dice (A,B) = 2(intersected region)/(sum of region A and region B) (Zou, et al., 2004)

If one of the patient's connectivity patterns matches that of a known network, then it will have a high Dice coefficient for that network and a low Dice coefficient for the rest. A good match (spatial overlap) occurs when the Dice coefficient is greater than 0.7, and if the Dice coefficient is less than 0.4 the overlap is considered poor (Zou, et al., 2004). For the purposes of this research, any intermediate values ($0.5 < \text{value} < 0.7$) will be reported as inconclusive, so the doctor or caregiver can examine them further. The algorithm is written in MATLAB.

The algorithm will accept an input data set for the patient, an input normative data set for each of 4 known connectivity networks (default mode, motor, vision, and auditory), and an optional mask input data set (to restrict the Dice comparison to certain areas of the brain so as to reduce computation time). The algorithm will then perform the spatial comparison and return the Dice coefficient of how well the patient data matches the normative connectivity patterns. The data will be output into a table so the Dice coefficient for each comparison can be displayed clearly, and then the whole table would repeat for each patient ICN. The table will show how well the patient's connectivity matches each of the normative patterns and in the comment section will outline what the Dice coefficient likely means (i.e. if the patient's connectivity is likely a match to motor, default, auditory, or visual). If there is a strong pattern of connectivity in the patient that does <u>not</u> correlate strongly with any of the known networks, it is likely to be aberrant (as in the above example) and is so marked in the table.

CHAPTER IV

RESULTS

A. Normative Dataset

The normative connectivity patterns, reflecting the degree of temporal correlation of the resting state fMRI signals for voxels within each network, from the 3 subjects chosen from the HCP data are shown in Figure 15 a) – d). The normative connectivity data set is the spatial average of the 3 subjects.

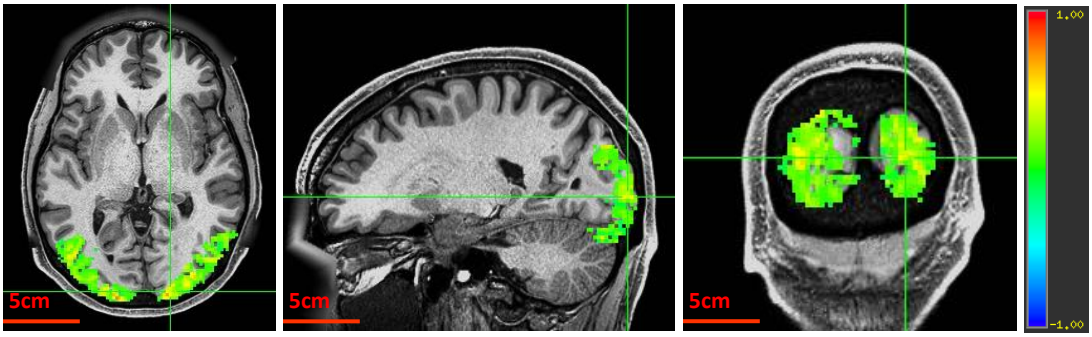

Axial view Sagittal view Coronal view

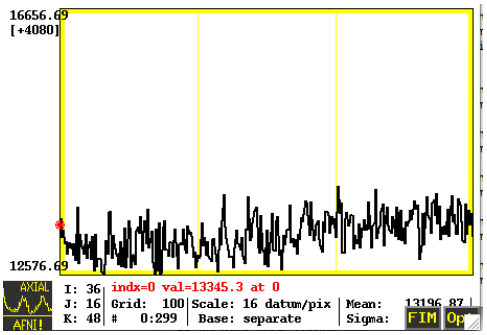

Time course

a) Normative vision data set

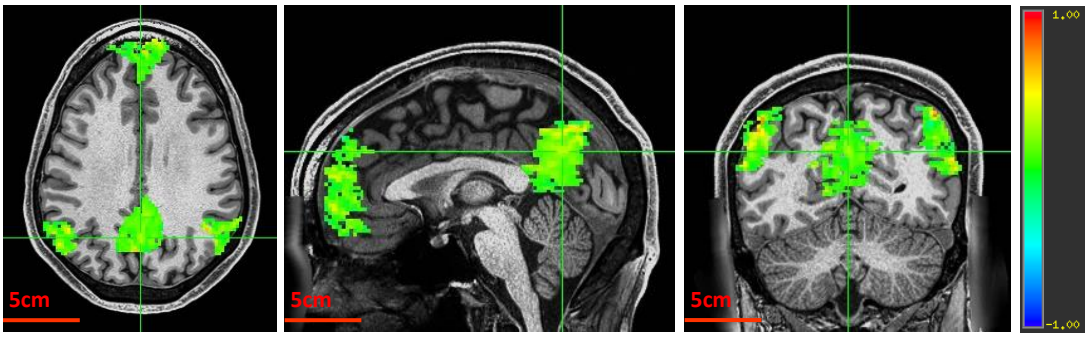

Axial view Sagittal view Coronal view

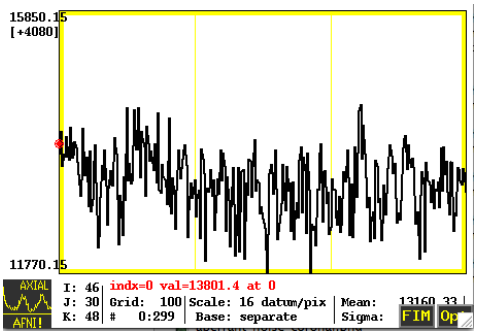

Time course

b) Normative default mode data set

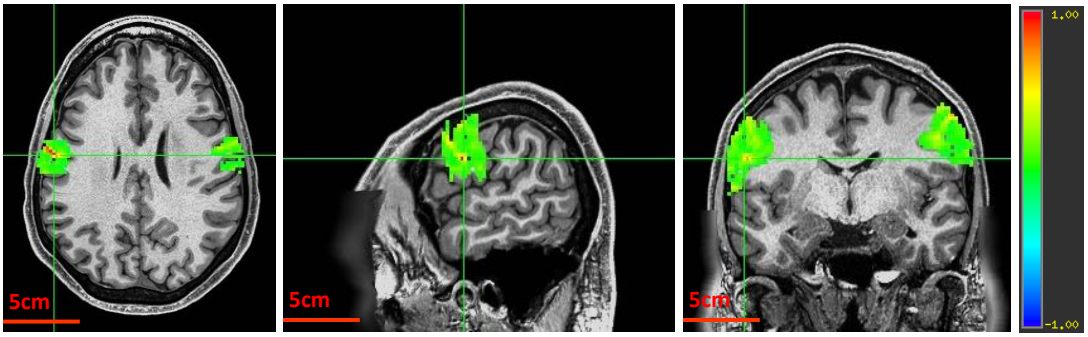

Axial view Sagittal view Coronal view

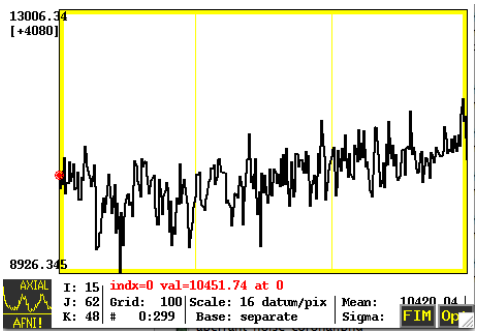

Time course

c) Normative auditory data set

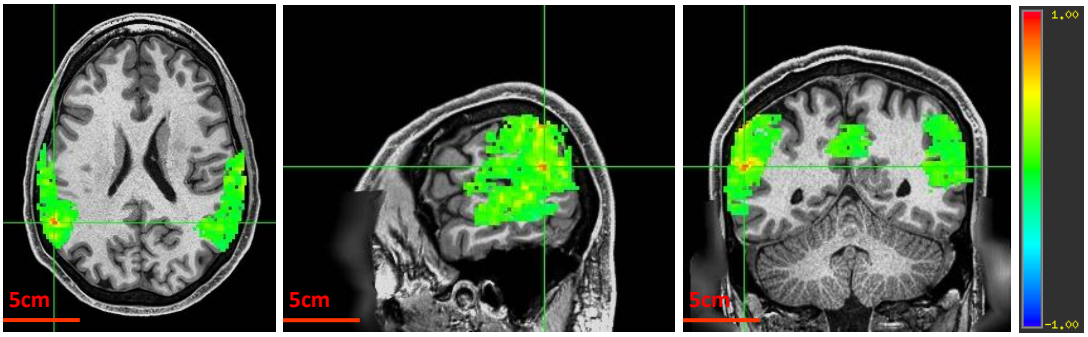

Axial view Sagittal view Coronal view

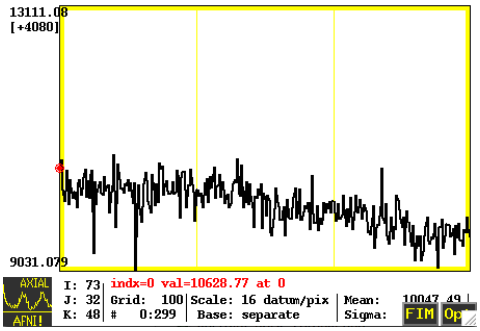

Time course

d) Normative motor data set

Figure 15: The normative data sets for the 4 brain regions chosen (a) vision b) default mode c) auditory d) motor), with axial, sagittal, and coronal views from left to right.

The normative data sets for vision, default mode, auditory, and motor functional areas were spatially averaged and match the known connectivity patterns for healthy individuals found in the previous research and literature (Shirer et al., 2012). They are broader (i.e. have larger areas of activation) since there are multiple subjects averaged together, but this is expected when compared to a single subject's activation since there is more variation when multiple subjects are considered, and additionally since the averages were computed spatially, the spread may be due to individual variations in brain structure and function (anatomical, functional, etc). This makes the spatially averaged activation patterns good for comparing individual subject data because small variations (anatomical, etc) in individual brains will be accommodated by the normative data set. The motor data

set is the most different from an individual subject motor connectivity pattern, but this is again due to the higher variability and also because the motor pattern is one of the more difficult ones for the Melodic ICA to distinguish (meaning that the SNR is lower). All 4 group data sets were successfully created and can be used in the biomarker algorithm. The group data sets can be used in future research as well since they are actual subject data, the number of subjects included can be increased as well to create a larger normative data set.

B. Simulated Aberrant Connectivity

The simulated aberrant connectivity pattern caused by mTLE is shown in Figure 16. The activation pattern was successfully created and detected when the data set was processed through Melodic ICA.

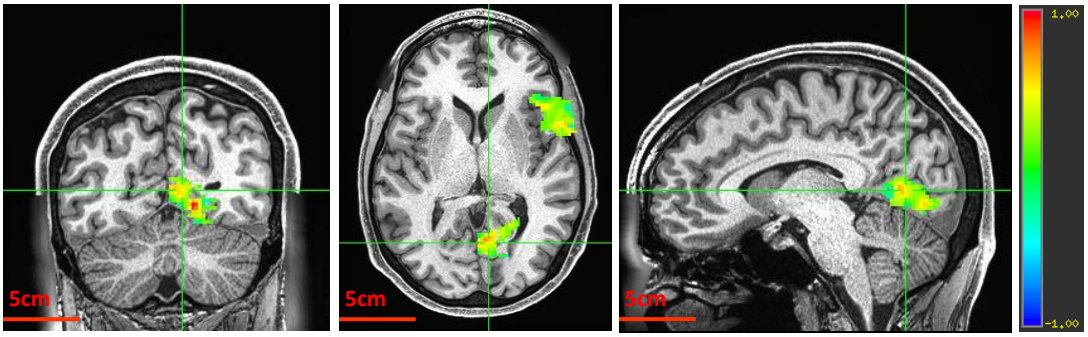

Axial Sagittal Coronal

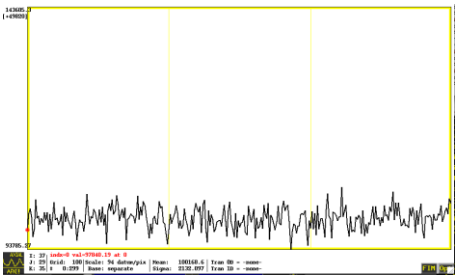

Time course

Figure 16: The simulated aberrant connectivity in the medial temporal and frontal lobe due to mTLE including the time course graph.

The simulated connectivity pattern matches previously published patterns for mTLE patients, and it is a critical first step in testing and verifying the biomarker algorithm. By using the simulated connectivity shown in Figure 16, a clean and known connectivity pattern can be used to verify the effectiveness of the algorithm under ideal conditions and also to debug the algorithm. This is critical because it verifies that the algorithm is working correctly, making it easier to move forward in the future into testing with actual patient data (if the algorithm was not tested this way first, it would be extremely difficult to debug and verify it).

C. Noise and Signal Level Sensitivity

The noise added to the aberrant connectivity signal was Gaussian temporal noise and was spatially distributed as shown in Figure 17.

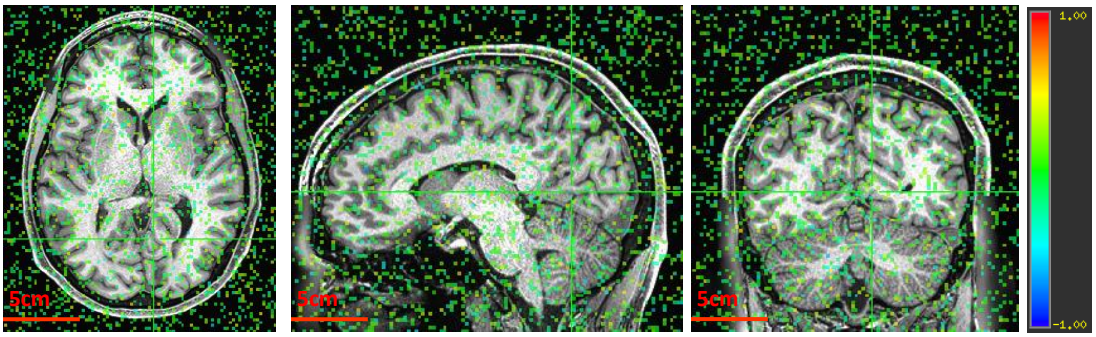

Axial Sagittal Coronal

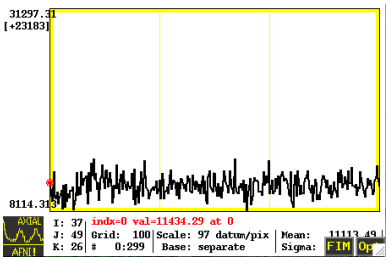

Time course

Figure 17: The Gaussian noise added to the aberrant connectivity

The Gaussian noise simulates the noise present in every physiological signal and the noise seen in Figure 17 is added to the aberrant connectivity signal in Figure 16 by a simple addition command in AFNI. This much more accurately simulates a physiological connectivity pattern. The noise added to the aberrant connectivity is shown in Figure 18. In this example, the noise was added everywhere, but ideally it would be restricted to just the voxels in the brain area that have noise levels higher than voxels outside the brain.

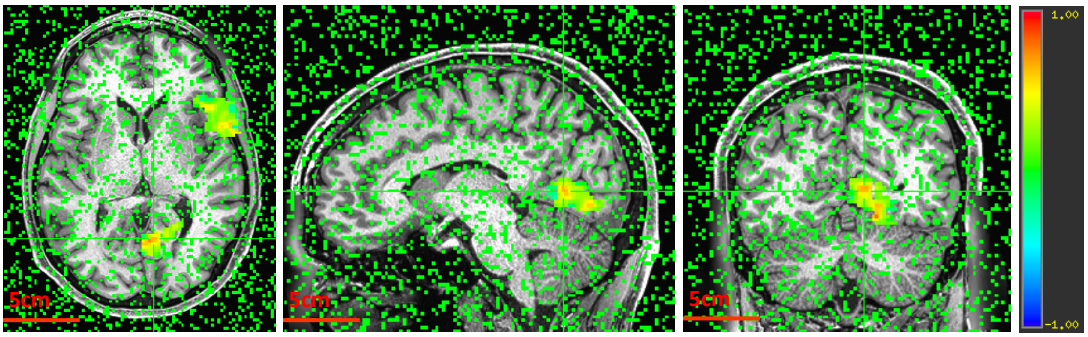

Axial Sagittal Coronal

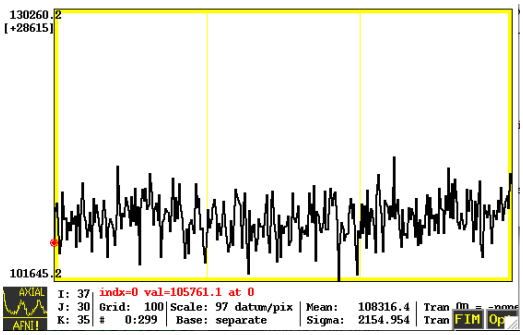

Time course

Figure 18: The Gaussian noise added to the aberrant connectivity

The signal level was also changed from having a constant amplitude to having a varying amplitude with the center of activation having higher correlation and the edges having lower correlation (See Chapter III, Section D for further detail) and is shown in Figure 19.

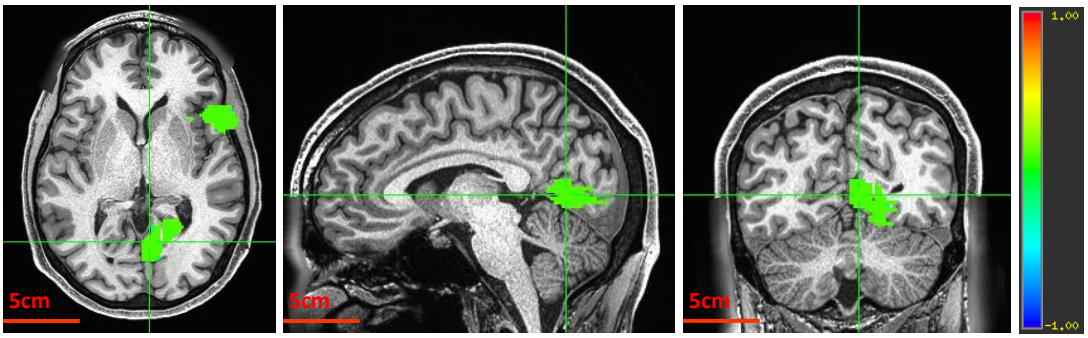

Axial Sagittal Coronal

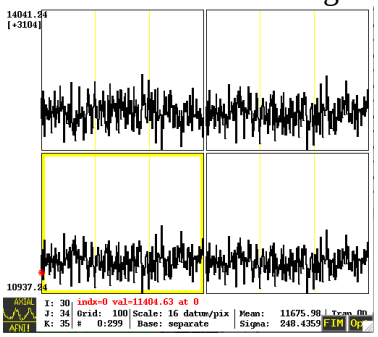

Time course

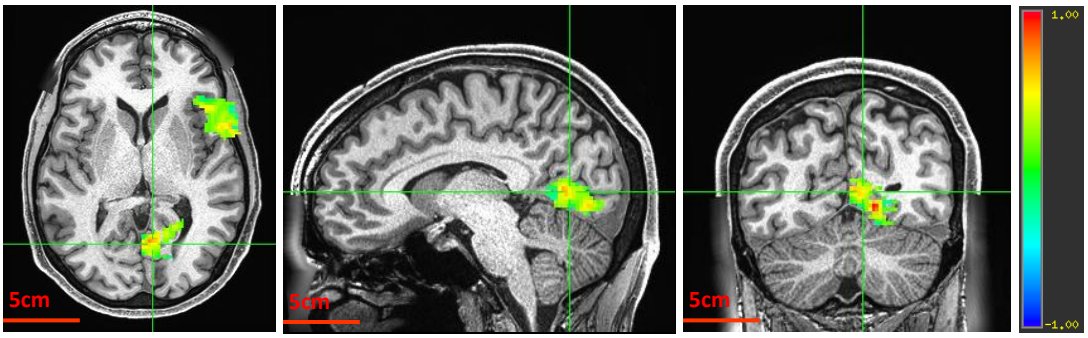

Axial Sagittal Coronal

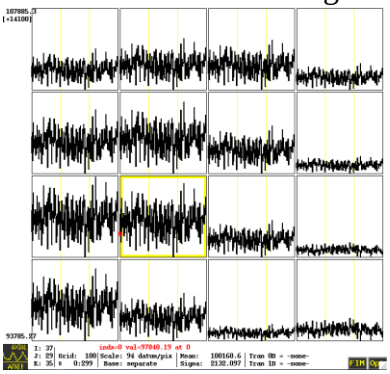

Time course

Figure 19: The signal level before (top) and after (middle) it was changed from having constant amplitude to having higher amplitude in the center and lower at the edges. The time course graph shows the change in amplitude of the time course.

As seen in Figure 19, the signal after the signal level was changed from a uniform level to a physiologically accurate level can be seen in the varying colors (from green to red, 0 to 1) with green showing the lower amplitude regions and red showing the higher amplitude regions. The red at the center of the activation areas shows the highest level of activation, while the edges are green showing a lower level of activation. This is further confirmed by the time course graph, which shows the high amplitude of the time course in the voxels at the center of the activation pattern and the voxels at the edge are lower amplitude. This makes the spatial pattern of simulated aberrant connectivity more physiologically accurate. The final simulated aberrant connectivity pattern used in the biomarker algorithm is the most accurate and most closely matches the form of the connectivity patterns from previous literature (Biswal et al., 1995; Lee et al, 2012), with varying signal level intensity and Gaussian noise included. Finally, since physiological noise varies in amplitude, the amplitude of the Gaussian noise was changed to 8 different levels to quantify the effectiveness of the biomarker algorithm on signals with various amounts of noise. These results are shown in Section D below.

D. The Biomarker Algorithm

First, the biomarker algorithm was tested by comparing the connectivity patterns from the 4 known activation patterns to the normative data sets (so default was compared to default, motor to motor, etc). If the algorithm is working correctly, the Dice coefficients should be close to one. The biomarker algorithm was also used to compare the simulated aberrant connectivity pattern to each of the 4 brain activation regions in the

normative database, and the Dice coefficients should be low. The Dice coefficient was the output for each of the comparisons, and the results are summarized in Table 1.

Table 1: The biomarker algorithm Dice comparison between individual patient connectivity from the auditory, default, motor, and visual activation regions to their corresponding normative databases.

Patient Connectivity	**Normative Brain Region**	**Dice Coefficient**	**Comments**
Default	Default	0.92 $\pm$ 0.065	High Dice coefficient, patient connectivity is likely default
Motor	Motor	0.90 $\pm$ 0.060	High Dice coefficient, patient connectivity is likely motor
Auditory	Auditory	0.89 $\pm$ 0.057	High Dice coefficient, patient connectivity is likely auditory
Visual	Visual	0.92 $\pm$ 0.035	High Dice coefficient, patient connectivity is likely visual
mTLE	Default	0.36 $\pm$ 0.026	Low Dice coefficient, patient connectivity is not likely default
mTLE	Motor	0.49 $\pm$ 0.015	Low Dice coefficient, patient connectivity is not likely motor
mTLE	Auditory	0.45 $\pm$ 0.026	Low Dice coefficient, patient connectivity is not likely auditory
mTLE	Visual	0.51 $\pm$ 0.007	Intermittent Dice coefficient, patient connectivity may be aberrant
mTLE connectivity is potentially aberrant - no good match with known ICNs.			

As seen in Table 1, the aberrant connectivity pattern did not match any of the 4 known activation patterns from the auditory, default, motor, or visual brain regions since the Dice coefficients were low (0.50 or lower). An unpaired T test was performed of the averaged of the matched versus the average of the unmatched components, with $p < 0.05$

being statistically significant. The result of the test was p = 0.0002, further confirming that the difference between the aberrant connectivity pattern and the known connectivity patterns is statistically significant. This means that the simulated aberrant connectivity pattern being matched was correctly identified as potentially aberrant because it does not match a known connectivity pattern. While this testing shows that the algorithm is working correctly, the effectiveness (sensitivity and specificity) of the algorithm when noise is included in the physiological signal must be quantified. To do this, the amplitude of the Gaussian noise was changed to 8 different levels and added to the simulated aberrant connectivity, and then the biomarker algorithm run on each of the 8 data sets to get the Dice coefficient. When the signal to noise ratio (SNR) is high, the Dice coefficient should be high, and as the noise amplitude increases, the SNR and Dice coefficient should both decrease. The relationship is quantified and shown in Figure 20.

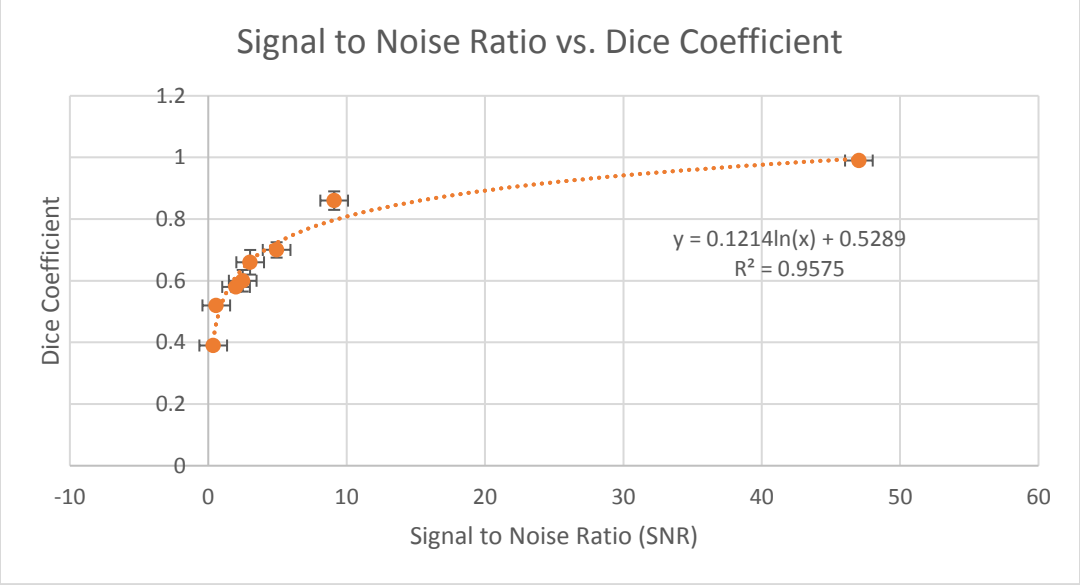

Figure 20: The signal to noise ratio vs the Dice coefficient as the noise level in the rsfMRI signal is increased.

This relationship between noise and the Dice coefficient is a critical step in quantifying the biomarker algorithm. According to this curve, the minimum acceptable SNR to avoid misclassification of ICNs is 4.1 (obtained by solving the equation of the curve for the SNR with a Dice coefficient of 0.7). The biomarker algorithm also returns the amount of true positives, true negatives, false positives, and false negatives, so the sensitivity and specificity of the algorithm can be calculated for any signal based on its SNR. These measures are shown graphically in Figures 21 and 22.

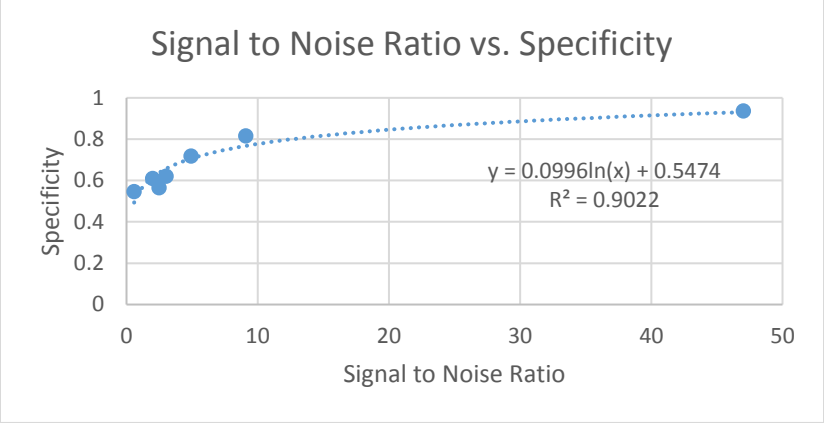

Figure 21: The Signal to Noise Ratio vs Specificity as the noise level in the rsfMRI signal is increased

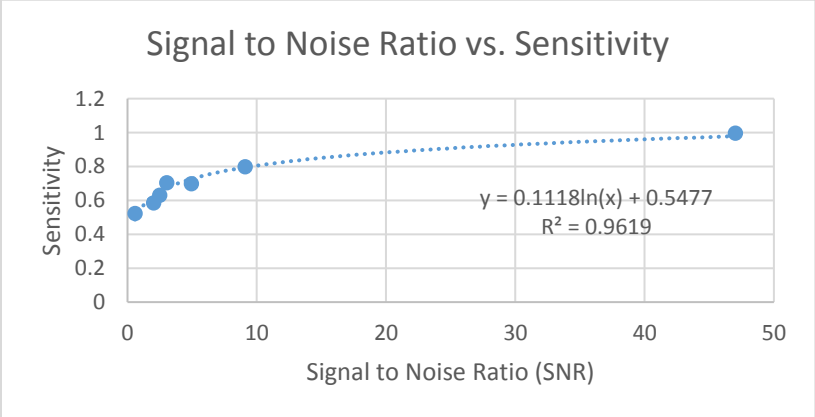

Figure 22: The Signal to Noise Ratio vs Sensitivity as the noise level in the rsfMRI signal is increased

For example, when the SNR is at 9, the sensitivity is 0.80 and the specificity is 0.82. With the three curves (obtained from the biomarker algorithm) shown in Figures 20, 21, and 22, the Dice coefficient, sensitivity, and specificity can be calculated for any level of SNR in the rsfMRI signal (Altman, et al, 1994).

CHAPTER V

DISCUSSION

A. Significance in Single Subject Data Evaluation

This research is significant in moving rsfMRI towards use in a clinical setting for individual patients. In order to be useful in a clinical setting, clinicians and doctors must have a statistically verified method to compare individual patients to a healthy normative group database, and a clinical tool to perform the comparison so they no longer have to manually inspect the connectivity patterns to identify aberrant patterns. In this project we developed a biomarker algorithm suitable for use as a clinical tool for doctors. The algorithm was verified using single subject simulated data and comparing it to a healthy normative group database, and it successfully identified the simulated connectivity as aberrant by producing Dice coefficients lower than 0.5 when the simulated connectivity was compared to the normative database. When 2 data sets were compared that were the same, the Dice coefficient came out close to one, proving that the algorithm is working correctly. Additionally, the relationship between the Dice coefficients and the level of noise present in the signal (SNR) was quantified by running the biomarker algorithm on 8 data sets, ranging from no noise to pure Gaussian noise, and obtaining the Dice coefficient for each set. This relationship is quantified by the equation $y = 0.1214\ln(x) + 0.5289$ where y is the Dice coefficient and x is the SNR. While the program cannot make patient care decisions, it can return comments on whether the Dice coefficient appears to show if a patient's connectivity pattern is aberrant. This successful application of the biomarker algorithm is a critical success in developing a clinical tool for use in a clinical

setting for individual patients. The normative database, simulated connectivity, and biomarker algorithm developed are a combination of advances toward the goal of making rsfMRI valuable for individual patients in a clinical setting.

B. Comparison to Previous Work

The aberrant connectivity pattern that was simulated was based on the activation regions that are affected by mTLE as shown in previous research. Moreover, the noise and signal levels also match the physiological form of connectivity patterns as also established by previous research. Previous work has also investigated abnormal connectivity patterns in epilepsy (Zhang, et al., 2009; Xu, et al., 2014) as well as cerebral structure changes as a biomarker of epilepsy (Woermann et al, 1999), and this work builds on the previous research. Additionally, Vergun et al. recently released a paper on using machine learning to classify spatial maps of resting state networks according to their overall function (Vergun, et al, 2016). Such an approach might be helpful in future work to refine the biomarker algorithm described here. It is important to note that the approach described here differs from previous work as it combines the Dice coefficient spatial matching technique with simulations of aberrant connectivity in order to test the algorithm's ability to accurately detect aberrant connectivity in single subjects rather than between groups.

Previous work identified the brain activation patterns corresponding to the auditory, default, motor, and visual networks for individuals (Shirer, et al, 2012 and Liu, et al, 2009), and the group normative dataset reported here for the 4 networks matches these areas based on qualitative visual analysis. Our group results differ in that the

activation areas are a bit broader (i.e. the activation area is larger), but this is partially due to the fact that there are multiple data sets averaged together. Since the activation patterns are not identical, the slight variations cause the broader group activation pattern. Also, cross-subject averaging, as was done here, increases sensitivity which can also broaden the activation areas. Additionally, there can be variations in the sulcal anatomy that may contribute to the broader activation patterns when averaging across brains. One approach that could help mitigate this problem would be to use a surface based registration system, which provides "a common spatial framework and a substrate for open-ended comparisons across data sets" (Van Essen, 2004), or using a parcellation approach to better align functional brain subdivisions between subjects (Glasser, et al., 2016).

C. Problems and Limitations

There are certainly limitations to this work that should be addressed if this research is to move forward in the future. One such limitation is the fact that only 4 regions of the brain were used (motor, default, vision, auditory) to perform the Dice statistical comparison between the patient and the normative database. While the 4 chosen represent 4 of the larger functional areas of the brain, there are fifteen plus other different, smaller regions that are also known. Expanding to more than the 4 areas would increase computation time for both the normative database and the algorithm's functionality and would likely alter the criteria for classifying a pattern as aberrant to some degree.

D. Future Work and Implications

Future work on this research should address the problems and limitations discussed in Section C. Certainly, moving to a larger and more random population of subject data can be used to create a larger normative data set. The 3 subject normative data set, while effective as a first step, will only become more effective as more subjects are added to it as it will become more and more representative of an entire population, and also as more subjects are added, any outlying connectivity abnormalities that are not due to disease will be averaged out, creating a cleaner normative comparison. Recently released from the HCP is a large set of averaged ICN data from their patient pool, and future work would investigate using this large average set as the normative database. Ideally, the normative database would be set up so that as more healthy subject data was collected, it could simply be added to the existing normative database, and over time the healthy normative database would just grow larger and larger. This would decrease the effect of individual subject variations that occur naturally as they could be averaged out when combined with a much larger population. This averaging effect occurs with the HCP data set as well (which is the largest MRI data collection project to date), but it would only increase as the sample size increased. Of potential use in the future is a recent release from the HCP that has a group average of 900 subjects, with a group ICA analysis performed in Melodic on all 900 subjects. This 900 subject group average may be useful in the future in the biomarker algorithm for comparison to the aberrant connectivity.

Additionally, the algorithm and normative database could be expanded to include more than the 4 functional brain regions used here. The normative database would include all of the known functional areas (even the smaller ones) so the algorithm would be that much more accurate and potentially able to match even lower signal level aberrant

connectivity patterns. Obviously the current algorithm could make mistakes by indicating that a patient ICN is aberrant (does not match any of the tested normal patterns) but in fact matches a normal ICN that was not tested.

Future work with the algorithm would expand its functionality. Currently, the algorithm can perform the matching for the 4 different functional areas sequentially (one must be completed before the next can be performed). Ideally, the algorithm would be expanded to be able to perform the matching on all functional areas from the normative database simultaneously. This would make the input process for the user much easier. Additionally, it would be beneficial to add various display options, for example so the user could look at an overlay of the patient data vs. the normative data set.

Finally, to really use the algorithm in the future in a clinical setting, it must be verified using more aberrant connectivity patterns as well as actual patient aberrant connectivity patterns (instead of simulated). Further research and study would undoubtedly lead to using actual patient data in the algorithm once it has been proven to work with simulated data. Using actual patient data is an important step on the way to clinical application as it is what will be used in the algorithm on a daily basis in a clinical setting.

CHAPTER VI

CONCLUSION

The goal of this research was to develop a biomarker to detect aberrant brain connectivity in individual patients. It is critical for rsfMRI use in a clinical setting that an individual's connectivity pattern be evaluated on its own, without being averaged into a larger data set. Currently, research has been performed on clinical evaluations of group data, but no clinical tool exists to evaluate individuals. The research performed here seeks to advance previous research by developing a normative database, simulating an individual connectivity with an aberrant connectivity pattern, and using a biomarker algorithm to compare that individual's aberrant connectivity to the healthy normative database. A biomarker algorithm of this type has not yet been developed, so the research here is a critical step forward in individual patient connectivity evaluation.

The outcome of this work is a biomarker algorithm that accepts inputs of an individual patient's rsfMRI data and a normative database. The algorithm performs a spatial comparison of the 2 datasets and returns the Dice coefficient, with a Dice coefficient greater than 0.7 showing a statistically significant match between the 2 datasets. The biomarker algorithm developed here and the Dice comparison process used to do so is an important step forward in the research of making rsfMRI useful for individual patients in a clinical setting. It is an automated matching method, meaning that classifying the patient's connectivity pattern is automated and provides quantitative metrics of the goodness of match or lack of match to known healthy ICNs. This will save the clinician time, and expands the use of rsfMRI for clinical evaluations, which is also

important since rsfMRI is a valuable tool that is important especially for patients that can't accomplish a task based MRI (the elderly, epilepsy patients, etc).

The field of MRI research has grown by leaps and bounds, especially since it began to be used in a clinical setting. The importance of individual patient evaluation in a clinical setting has been established, and research is moving to make this a reality. The research performed here successfully developed a biomarker that detected an aberrant connectivity pattern that plausibly might be caused by mTLE in an individual patient and as such is an important step forward in rsfMRI research.

BIBLIOGRAPHY

Aertsen, A. M. H. J., Gerstein, G. L., Habib, M. K., & Palm, G. (1989) Dynamics of Neuronal Firing Correlation: Modulation of "Effective Connectivity." Journal of Neurophysiology, 61(5), 900 – 917. Retrieved February 2, 2016 from http://www.cnbc.cmu.edu/~samondjm/papers/Aertsenetal1989.pdf

Altman, D. G., & Bland, J. M. (1994) Diagnostic tests 1: sensitivity and specificity. BMJ, 308, 1552. Retrieved October 18, 2016 from https://www.ncbi.nlm.nih.gov/pmc/articles/PMC2540489/pdf/bmj00444-0038.pdf

Assaf, M., Jagannathan, K., Calhoun, V. D., Miller, L., Stevens, M. C., Sahl, R., O'Boyle, J. G., Schultz, R. T., & Pearlson, G. D. (2010) Abnormal functional connectivity of default mode sub-networks in autism spectrum disorder patients. NeuroImage, 53(1), 247 – 256. Retrieved January 20, 203216 from doi: 10.1016/j.neuroimage.2010.05.067

Beckmann, C. F., DeLuca, M., Devlin, J. T., & Smith, S. M. (2005) Investigations into resting-state connectivity using independent component analysis. Philosophical Transactions of the Royal Society, 360, 1001 – 1013. Retrieved March 1, 2016 from doi: 10.1098/rstb.2005.1634.

Beckman, C. F., Mackay, C. E., Filippini, N., & Smith, S. M. Group comparison of resting-state FMRI data using multi-subject ICA and dual regression. FMRIB Centre. Retrieved February 21, 2016 from http://fsl.fmrib.ox.ac.uk/fsl/fslwiki/DualRegression?action=AttachFile&do=get&target=CB09.pdf

Bell, A. J., & Sejnowski, T. J. (1995) An information-maximixation approach to blind separation and blind deconvolution. Neural Computation, 7(6), 1004 – 1034. Retrieved February 26, 2016 from http://www.inf.fu-berlin.de/lehre/WS05/Mustererkennung/infomax/infomax.pdf.

Bettus, G., Bartolomei, F., Confort-Gouny, S., Guedj, E., Chauvel, P., Cozzone, P. J., Ranjeva, J. P., & Guye, M. (2010) Role of resting state functional connectivity MRI in presurgical investigation of mesial temporal lobe epilepsy. Journal of Neurology, Neurosurgery & Psychiatry. Retrieved January 30, 2016 from doi: 10.1136/jnnp.2009.191460.

Biswal, B., Yetkin, F. Z., Haughton, V. M., & Hyde, J. S. (1995) Functional connectivity in the motor cortex of resting human brain using echo-planar mri. Magnetic Resonance in Medicine, 34(4), 537-541. Retrieved February 3, 2016 from https://www.researchgate.net/profile/Victor_Haughton/publication/51295687_Functional_connectivity_in_the_motor_cortex_resting_human_brain_using_echo-planar_MRI/links/0deec51d9c87190d28000000.pdf

Biswal, B., Kylen, J. V., & Hyde, J. S. (1997) Simultaneous Assessment of Flow and BOLD Signals in Resting-State Functional Connectivity Maps. NMR in Biomedicine, 10, 165 – 170. Retrieved January 29, 2016 from https://www.researchgate.net/profile/Bharat_Biswal/publication/13800770_Simultaneous_assessment_of_flow_and_BOLD_signals_in_resting-state_functional_connectivity_maps/links/004635338615f08e51000000.pdf

Biswal, B., & Ulmer, J. L. (1999) Blind source separation of multiple signal sources of fMRI data sets using independent component analysis. Journal of Computer Assisted Tomography, 23, 265 – 271. Retrieved February 22, 2016 from http://cds.ismrm.org/ismrm-1999/PDF6/1715.pdf

Biswal, B. (2012). Resting State fMRI: A Personal History. NeuroImage (2012), Retrieved January 14, 2016 from doi: 10.1016/j.neuroimage.2012.01.090

Calhoun, V. D., Adali, T., Pearlson, G. D., & Pekar, J. J. (2001) A Method for Making Group Inferences from Functional MRI Data Using Independent Component Analysis. Human Brain Mapping, 14, 140 – 151. Retrieved March 1, 2016 from http://www.nrciol.org/cores/mialab/personnel/calhoun/2001_HBM_GroupICA_reprint.pdf

Chodos, A. (Ed.). (2006). July, 1977: MRI Uses Fundamental Physics for Clinical Diagnosis. American Physical Society, 15(7). Retrieved January 17, 2016, from https://www.aps.org/publications/apsnews/200607/history.cfm

Chou, Y. H., Panych, L. P., Dickey, C. C., Petrella, J. R., & Chen, N. K. (2012) Investigation of Long-Term Reproducibility of Intrinsic Connectivity Network Mapping: A Resting-State fMRI study. American Journal of Neuroradiology, 33, 833 – 838. Retrieved February 15, 2016 from doi: 10.3174/ajnr.A2894.

Comon, P. (1992) Independent component analysis, A new concept. Signal Processing, 36, 287 – 314. Retrieved January 31, 2016 from http://www.ece.ucsb.edu/wcsl/courses/ECE594/594C_F10Madhow/comon94.pdf

De Luca, M., Beckmann, C. F., De Stefano, N., Matthews, P. M., & Smith, S. M. (2005) fMRI resting state networks define distinct modes of long-distance interactions in the human brain. Neuroimage, 29(4), 1359-1367. Retrieved January 18, 2016 from doi: 10.1016/j.neuroimage.2005.08.035

Dimmock, M. (2013, September 26). The science of medical imaging: Magnetic resonance imaging (MRI). Retrieved January 12, 2016, from http://theconversation.com/the-science-of-medical-imaging-magnetic-resonance-imaging-mri-15030

Fox, M. D., & Greicius, M., (2010) Clinical applications of resting state functional connectivity. Frontiers in Systems Neuroscience, 4(19), 1 – 9. Retrieved January 23, 2016 from doi: 10.3389/fnsys.2010.00019.

Friston, K. J. (2011) Functional and Effective Connectivity: A Review. Brain Connectivity, 1(1), 13 – 36. Retrieved July 26, 2016 from doi: 10.1089/brain.2011.0008.

Geva, T., MD. (2006). Magnetic Resonance Imaging: Historical Perspective. Journal of Cardiovascular Magnetic Resonance, 8, 573-580. Retrieved January 11, 2016, From http://www.scmr.org/assets/files/members/documents/JCMR/008/LCMR_i_008_04_tfja/LCMR_i_8_04_O/LCMR_A_175489_O.pdf

Greicius, M. (2008) Resting-state functional connectivity in neuropsychiatric disorders. Current Opinion in Neurology, 21, 424-430. Retrieved January 22, 2016 from http://findlab.stanford.edu/Publications/Greicius%202008%20-%20Curr%20Opin%20Neurol.pdf

Greicius, M. D., Supekar, K., Menon, V., & Dougherty, R. F. (2009) Resting-State Functional Connectivity Reflects Structural Connectivity in the Default Mode Network. Cerebral Cortex, 19(1), 72-78. Retrieved January 22, 2016 from doi: 10.1093/cercor/bhn059

Glasser, M. F., Coalson, T. S., Robinson, E. C., Hacker, C. D., Harwell, J., Yacoub, E., Ugurbil, K., Andersson, J., Beckmann, C. F., Jenkinson, M., Smith, S. M. & Van Essen, D. C. (2016) A multi-modal parcellation of human cerebral cortex. Nature, 536, 171 – 178. Retrieved October 7, 2016 from doi: 10.1038/nature18933.

Hampson, M., Peterson, B. S., Skudlarski, P., Gatenby, J. C., & Gore, J. C. (2002) Detection of functional connectivity using temporal correlations in MR images. Human Brain Mapping, 15(4), 247-262. Retrieved January 27, 2016 from doi: 10.1002/hbm.10022.

Humandiagram.info. (2016). Brain Anatomy that Controls Our Body. Retrieved March 15, 2016 from http://humandiagram.info/brain-anatomy-that-controls-our-body/.

Jenkinson, Mark. (2013) FSL Melodic. Retrieved August 27, 2016 from http://fsl.fmrib.ox.ac.uk/fsl/fslwiki/MELODIC

Kim, M. J. J., Holodny, A. I., Hou, B. L., Peck, K. K., Moskowitz, C. S., Bogomolny, D. L., & Gutin, P. H. (2005) The Effect of Prior Surgery on Blood Oxygen Level Dependent Functional MR Imaging In the Preoperative Assessment of Brain Tumors. American Journal Of Neuroradiology, 26, 1980 – 1985. Retrieved January 28, 2016 from http://www.ajnr.org/content/26/8/1980.full.pdf+html

Krings, T., Reinges, M. H. T., Erberich, S., Kemeny, S., Rohde, V., Spetzger, U., Korinth, M., Willmes, K., Gilsbach, J. M., & Thron, A. (2001) Functional MRI for presurgical planning: problems, artifacts, and solution strategies. J Neurol Neurosurg Psychiatry, 70, 749 – 760. Retrieved January 29, 2016 from http://jnnp.bmj.com/content/70/6/749.full.pdf+html

Lee, C. C., Ward, H. A., Sharbrough, F. W., Meyer, F. B., Marsh, R. W., Raffel, C., So, E. L., Cascino, G. D., Shin, C., Xu, Y., Riederer, S. J., Jack, C. R. (1999) Assessment of Functional MR Imaging in Neurosurgical Planning. American Journal Of Neuroradiology, 20, 1511 – 1519. Retrieved January 27, 2016 from doi: http://www.ajnr.org/content/20/8/1511.long

Lee, M. H., Smyser, C. D., & Shimonya, J. S. (2012) Resting-State fMRI: A Review of Methods and Clinical Applications. American Journal of Neuroradiology, 34, 1866 – 1872. Retrieved January 22, 2016 from doi: 10.3174/ajnr.A3263.

Liao, W., Zhang, Z., Pan, Z., Mantini, D., Ding, J., Duan, X., Luo, C., Lu, G., & Chen, H. (2010) Altered Functional Connectivity and Small-World in Mesial Temporal Lobe Epilepsy. PLOS One. Retrieved March 2, 2016 from http://dx.doi.org/10.1371/journal.pone.0008525.

Liu, H., Buckner, R. L., Talukdar, T., Tanaka, N., Madsen, J. R., & Stufflebeam, S. M. (2009) Task-free presurgical mapping using functional magnetic resonance imaging intrinsic activity. Journal of Neurosurgery, 111(4), 746 – 754. Retrieved January 29, 2016 from doi: 10.3171/2008.10.JNS08846.

Liu, W., Awate, S. P., & Fletcher, P. T. (2012) Group Analysis of Resting-State fMRI by Hierarchical Markov Random Fields. LNCS, 7512, 189 – 196. Retrieved February 17, 2016 from http://www.sci.utah.edu/~weiliu/publications/hiermrf_miccai12.pdf

Matthews, P. M., Honey, G. D., & Bullmore, E. T. (2006) Applications of fMRI in translational medicine and clinical practice. Nature Reviews Neuroscience, 7, 732-744. Retrieved January 24, 2016 from doi: 10.1038/nrn1929.

Mazziotta, J., Toga, A., Evans, A., Fox, P., Lancaster, J., Zilles, K., Woods, R., Paus, T., Simson, G., Pike, B., Holmes, C., Collins, L., Thompson, P., MacDonald, D., Iacoboni, M., Schormann, T., Amunts, K., Palomero-Gallagher, N., Geyer, S., Parsons, L., Narr, K., Kabani, N., LeGoualher, G., Boomsma, D., Cannon, T., Kawashima, R., & Mazoyer, B. (2001) A probabilistic atlas and reference system for the human brain: International Consortium for Brain Mapping (ICBM). The Royal Society, 356, 1293 – 1322. Retrieved August 15, 2016 from doi: 10.1098/rstb.2001.0915.

Nishimura, D. G. (1996). Principles of Magnetic Resonance Imaging (1st ed., Vol. 1). Stanford, CA: Stanford University.

Ogawa, S., Lee, T. M., Kay, A. R., & Tank, D.W. (1990). Brain magnetic resonance imaging with contrast dependent on blood oxygenation. Proc. Natl. Acad. Sci. USA. 87, 9868-9872. Retrieved January 16, 2016 from http://www.ncbi.nlm.nih.gov/pmc/articles/PMC55275/pdf/pnas01049-0370.pdf

Ogawa, S. & Sung, Y. (2007) Functional magnetic resonance imaging. Scholarpedia 2(10). Retrieved January 15, 2016 from doi: 10.4249/scholarpedia.3105

Pauling, L & Coryell C.D. (1936) The magnetic properties and structure of hemoglobin, oxyhemoglobin and carbonmonoxyhemoblobin. Proc. Natl. Acad. Sci. 22, 210-216. Retrieved January 15, 2016 from http://www.ncbi.nlm.nih.gov/Pmc/articles/PMC1076743/pdf/pnas01768-0018.pdf

Pereira, F., Mitchell, T., & Botvinick, M. (2009) Machine learning classifiers and fMRI: a tutorial overview. NeuroImage, 45, 199-209. Retrieved August 21, 2015 from doi: 10.1016/j.neuroimage.2008.11.007

Raichle, M. E., & Snyder, A. Z. (2007) A default mode of brain function: a brief history of an evolving idea. NeuroImage, 37, 1083 – 1090. Retrieved January 25, 2016 from doi: 10.1016/j.neuroimage.2007.02.041.

Raichle, M. E. (2008) A brief history of human functional brain mapping. Trends in Neurosciences, 32(2), 118-126. Retrieved January 24, 2016 from doi: 10.1016/j.tins.2008/11/001.

Roguin, A. (2004), Nikola Tesla: The man behind the magnetic field unit. Journal of Magnetic Resonance Imaging, 19, 369–374. Retrieved January 11, 2016, from doi:10.1002/jmri.20002

Shirer, W. R., Ryali, S., Rykhlevskaia, E., Menon, V., & Greicius, M. D. (2012). Decoding Subject-Driven Cognitive States with Whole-Brain Connectivity Patterns. Cerebral Cortex, 22(1), 1-8. Retrieved January 17, 2016, from doi: 10.1093/cercor/bhr099

Su, L., An, J., Ma, Q., Qiu, S., & Hu, D. (2015) Influence of Resting-State Network on Lateralization of Functional Connectivity in Mesial Temporal Lobe Epilepsy. American Journal of Neuroradiology, 36(8) 1479 – 1487. Retrieved February 1, 2016 from doi: 10.3174/ajnr.A4346.

Tubridy, N (2000). Neuroradiological history: Sir Joseph Larmor and the basis of MRI physics. Neuroradiology, 42, 852–5. Retrieved January 12, 2016 from http://www.ncbi.nlm.nih.gov/pubmed/11151696

Van den Heuvel, M. P., Hulshoff Pol, H. E. (2010) Exploring the brain network: A review on resting-state fMRI functional connectivity. European

Neuropsychopharmacology, 20 (8), 519 – 534. Retrieved February 6, 2016 from doi: 10.1016/j.euroneuro.2010.03.008.

Van de Ven, V. G., Formisano, E., Prvulovic, D., Roeder, C. H., & Linden, D. E. J. (2004) Functional Connectivity as Revealed by Spatial Independent Component Analysis of fMRI Measurements During Rest. Human Brain Mapping, 22, 165 – 178. Retrieved March 1, 2016 from doi: 10.1002/hbm.20022.

Van Essen, D. C. (2004) Surface-based approaches to spatial localization and registration in primate cerebral cortex. NeuroImage, 23, 97 – 107. Retrieved October 4, 2016 from doi: 10.1016/j.neuroimage.2004.07.024.

Van Essen, D. C., Smith, S. M., Barch, D. M., Behrens, T. E. J., Yacoub, E., Ugurbil, K. (2012). The WU-Minn Human Connectome Project: An overview. NeuroImage, 80, 62 – 79. Retrieved February 13, 2016 from doi: 10.1016/j.neuroimage.2012.02.018

Van Essen, D. c. (2016, January 14). The Human Connectome Project. Retrieved January 20, 2016, from http://www.humanconnectome.org/

Vergun, S., Gaggl, W., Nair, V. A., Suhonen, J. I., Birn, R. M., Ahmed, A. S., Meyerand, M. E., Reuss, J., DeYoe, E. A., & Prabhakaran, V. (2016) Classification and Extraction of Resting State Networks Using Healthy and Epilepsy fMRI Data. Frontiers in Neuroscience. Retrieved October 7, 2016 from http://dx.doi.org/10.3389/fnins.2016.00440.

Voets, N. L., Beckmann, C. F., Cole, D. M., Hong, S., Bernasconi, A., & Bernasconi, N. (2012) Structural substrates for a resting network disruption in temporal lobe epilepsy. Brain: A Journal of Neurology, 137, 2350 – 2357. Retrieved February 5, 2016 from doi: http://dx.doi.org/10.1093/brain/aws.

Weissenbacher, A., Kasess, C., Gerstl, F., Lanzenberger, R., Moser, E., & Windischberger, C. (2009) Correlations and anticorrelations in resting-state functional connectivity MRI: A quantitative comparison of preprocessing strategies. NeuroImage, 47(4), 1408 – 1416. Retrieved January 26, 2016 from doi: 10.1016/j.neuroimage.2009.05.005.

Weng, S. J., Wiggins, J. L., Peltier, S. J., Carrasco, M., Risi, S., Lord, C., & Monk, C. S. (2010) Alterations of resting state functional connectivity in the default network in adolescents with autism spectrum disorders. Brain Research, 1313, 202-214. Retrieved January 21, 2016 from doi: 10.1016/j.brainres.2009.11.057.

Woermann, F. G., Free, S. L., Koepp, M. J., Sisodiya, S. M., & Duncan, J. S. (1999) Abnormal cerebral structure in juvenile myoclonic epilepsy demonstrated with voxel based analysis of MRI. Brain: A Journal of Neurology, 2101 – 2108. Retrieved October 7, 2016 from http://dx.doi.org/10.1093/brain/122.11.2101

Xu, Q., Zhang, Z., Liao, W., Xiang, L., Yang, F., Wang, Z., Chen, G., Tan, Q., Jiao, Q., & Lu, G. (2014) Time-Shift Homotopic Connectivity in Mesial Temporal Lobe Epilepsy. American Journal of Neuroradiology, 35, 1746 – 1752. Retrieved February 4, 2016 from doi: 10.3174/ajnr.A3934.

Zalesky, A., Fornito, A., & Bullmore, E. (2012) On the use of correlation as a measure of network connectivity. NeuroImage, 60(4), 2096 – 2106. Retrieved January 20, 2016 from doi: 10.1016/j.neuroimage.2012.02.001

Zhang, Z., Lu, G., Zhong, Y., Tan, Q., Yang, Z., Liao, W., Chen, Z., Shi, J., & Liu, Y. (2009) Impaired attention network in temporal lobe epilepsy: A resting FMRI study. Neuroscience letters, 458(3), 97-101. Retrieved January 26, 2016 from doi: 10.1016/j.neulet.2009.04.040.

Zhang, H. Y., Want, S. J., Liu, B., Ma, Z. L., Yang, M., Zhang, Z. J., & Teng, G. J. (2010). Resting Brain Connectivity: Changes during the Progress of Alzheimer Disease. RSNA Radiology, 256(2). Retrieved January 19, 2016 from doi: http://dx.doi.org/10.1148/radiol.10091701

Zou, K. H., Warfield, S. K., Bharatha, A., Tempany, C. M. C., Kaus, M. R., Haker, S. J., Wells, III, W. M., Jolesz, F. A., & Kikinis, R. (2004) Statistical Validation of Image Segmentation Quality Based on a Spatial Overlap Index. Acad Radiol. 11(2), 178 – 189. Retrieved March 17, 2016 from doi: 10.1016/S1076-6332(03)00671-8.

Appendix A

The spatial averaging code. Note that this code was used to spatially average each of the 4 brain regions (motor, vision, default, auditory) individually.

```
#!/bin/csh -f

####
#@break-up - breaks up and afni brink into the wanted sub-briks and then glues them back together into one afni brik.
## Note: subriks start at 0 while the compenets in melodic FSL do not, so you need to subtract one from the fsl compinenet number to get the correct afni subrik
### This code was adapted with permission and assistance from Jedediah Mathis (MCW).
####

#Variables

set ec = 'CFQ'
set task = 'melodic_IC_auto'
## Subbrik selection. These are the manually identified ICN's that correspond to motor, default, auditory, or vision
set sub1 = '2'
set sub2 = '4'
set sub3 = '9'
set sub4 = '10'

## Label new subriks with appropriate descriptor (labeling the chosen sub-briks
set subn1 = 'IC 2'
set subn2 = 'IC 4'
set subn3 = 'IC 9'
set subn4 = 'IC 10'

# Set the prefix label to identify the file once it has been averaged. Uncomment the appropriate prefix based on what brain region is being averaged
set prefix = 'melodic_IC-sub'
#set prefixf = 'melodic_Motor_IC'
#set prefixf = 'melodic_Default_IC'
#set prefixf = 'melodic_Auditory_IC'
set prefixf = 'melodic_Vision_IC'

cd afni

# Attach the prefix to each sub-brik
3dcopy {$task}.nii.gz {$task}+orig
3dcalc -a {$task}'+orig['{$sub1}']' -prefix {$prefix}{$sub1} -expr 'a'
3dcalc -a {$task}'+orig['{$sub2}']' -prefix {$prefix}{$sub2} -expr 'a'
3dcalc -a {$task}'+orig['{$sub3}']' -prefix {$prefix}{$sub3} -expr 'a'
```

```
3dcalc -a {$task}'+orig['{$sub4}']' -prefix {$prefix}{$sub4} -expr 'a'


3drefit -sublabel 0 {$subn1} {$prefix}{$sub1}+orig
3drefit -sublabel 0 {$subn2} {$prefix}{$sub2}+orig
3drefit -sublabel 0 {$subn3} {$prefix}{$sub3}+orig
3drefit -sublabel 0 {$subn4} {$prefix}{$sub4}+orig

# Spatially average the sub-briks together
3dmerge -gsmax -prefix {$prefixf}_merge {$prefix}{$sub1}+orig {$prefix}{$sub2}+orig
{$prefix}{$sub3}+orig {$prefix}{$sub4}+orig
```